

ARTICLE

mTORC2 suppresses cell death induced by hypo-osmotic stress by promoting sphingomyelin transport

Yumiko Ono¹, Kenji Matsuzawa¹, and Junichi Ikenouchi¹

Epithelial cells are constantly exposed to osmotic stress. The influx of water molecules into the cell in a hypo-osmotic environment increases plasma membrane tension as it rapidly expands. Therefore, the plasma membrane must be supplied with membrane lipids since expansion beyond its elastic limit will cause the cell to rupture. However, the molecular mechanism to maintain a constant plasma membrane tension is not known. In this study, we found that the apical membrane selectively expands when epithelial cells are exposed to hypo-osmotic stress. This requires the activation of mTORC2, which enhances the transport of secretory vesicles containing sphingomyelin, the major lipid of the apical membrane. We further show that the mTORC2–Rab35 axis plays an essential role in the defense against hypotonic stress by promoting the degradation of the actin cortex through the up-regulation of PI(4,5)P2 metabolism, which facilitates the apical tethering of sphingomyelin-loaded vesicles to relieve plasma membrane tension.

Introduction

Epithelial cells are exposed to interstitial fluid on the basement membrane side and to the external environment on the apical membrane side. While the basal membrane experiences an almost constant osmotic pressure (270–300 mOsm/liter), the apical membrane is perpetually exposed to osmotic stress because liquids of varying osmolarity exist in the external environment (fresh water, ~10 mOsm/liter; saliva, ~30 mOsm/liter).

In a hypo-osmotic environment, the influx of water molecules into the cell induces cell expansion and up-regulates plasma membrane tension. To prevent cell rupture, it is necessary to supply lipids to buffer the increased membrane tension (Pietuch et al., 2013). Several mechanisms to decrease the plasma membrane tension on hypotonic stress are reported (Pontes et al., 2017). First, the plasma membrane is reserved in the form of membrane folds that unfurl under tension to absorb the increase in cell volume. The invaginated membrane structure of the caveolae is a notable example, and it exerts a direct palliative effect against mechanical stress (Sinha et al., 2011). Second, exocytosis contributes to the expansion of the plasma membrane area by adding lipids; conversely, endocytosis arrest can also mitigate the effect of increased plasma membrane tension (Dai and Sheetz, 1995). On the other hand, increased membrane tension acts as an inhibitor of actin polymerization to reduce protrusive

membrane structures and cell surface area (Diz-Muñoz et al., 2016). However, the details of how these molecular mechanisms are coordinated in adapting to hypo-osmotic stress are unclear.

The apical membrane of the epithelial cells is enriched with sphingolipids, such as glycolipids and sphingomyelin (Gerl et al., 2012; Ikenouchi et al., 2012). We have shown that sphingolipids are abundant, especially in the microvilli of the apical membrane (Ikenouchi et al., 2013). In this study, we found that the apical membrane selectively expanded when epithelial cells were exposed to hypo-osmotic stress. This selective expansion of the apical membrane is caused by the enhanced transport of vesicles containing components of the apical membrane, such as sphingomyelin. Furthermore, we clarified that the mTORC2–Rab35 axis plays essential roles in adapting to hypo-osmotic stress by promoting apical transport to the supply membrane and by reducing the actin cortex to decrease plasma membrane tension.

Results

The morphological changes of epithelial cells induced by hypo-osmotic stress

The influx of water into cells upon exposure to hypo-osmotic fluids increases the cell volume and consequently the plasma

Department of Biology, Faculty of Sciences, Kyushu University, Nishi-ku, Fukuoka, Japan.

Correspondence to Junichi Ikenouchi: ikenouchi.junichi.033@m.kyushu-u.ac.jp.

© 2022 Ono et al. This article is distributed under the terms of an Attribution–Noncommercial–Share Alike–No Mirror Sites license for the first six months after the publication date (see <http://www.rupress.org/terms/>). After six months it is available under a Creative Commons License (Attribution–Noncommercial–Share Alike 4.0 International license, as described at <https://creativecommons.org/licenses/by-nc-sa/4.0/>).

membrane tension. To avoid rupture, cells must reduce membrane tension immediately. In most previous studies, molecular mechanisms of adaptation to hypo-osmotic stress were studied using non-epithelial cells that lack tight junctions (TJs), such as HeLa cells (Le Roux et al., 2019; Sinha et al., 2011). In the absence of TJs, the entire cell expands by disrupting invaginated membrane structures such as the caveolae, which functions as a reservoir of the plasma membrane (Kozera et al., 2009). Indeed, hypo-osmotic stress induces plasma membrane rupture in caveolin-deficient non-epithelial cells, such as fibroblasts or muscle fiber cells (Sinha et al., 2011).

Since epithelial cells are located on the surface of organs and exposed to drastic osmotic changes, we decided to investigate how they avoid cell death due to hypo-osmotic stress. We first sought to examine the source of the expanding membrane in the canine proximal tubule-derived epithelial cell line MDCK II. Apical and basolateral membranes were respectively visualized by staining for podocalyxin and E-cadherin. When MDCK II cells were exposed to a hypo-osmotic medium (150 mOsm/liter) from the apical side, the boundary between apical and basolateral membranes shifted to the basal side within 10 min (Fig. 1 A). We quantified the apical and basolateral surface areas and scored their relative enrichment under hypo-osmotic stress. The ratio of hypo-osmotic surface area (S_{Hypo}) to isotonic surface area (S_{Iso}) was increased only in the apical membrane, indicating that the expanding membrane is selectively derived from the apical membrane (Fig. 1 B). We also quantified the changes in the fluorescence intensities of E-cadherin (Fig. 1 C) and podocalyxin (Fig. 1 D). Strikingly, the fluorescence intensity of podocalyxin was not diluted by the surface area expansion, which suggests that there is a mechanism to rapidly deliver components of the apical membrane in response to the hypo-osmotic challenge (Fig. 1 D).

We wondered whether hypo-osmotic stress could trigger both apical membrane expansion and the delivery of apical membrane components to other epithelial cells. The mouse mammary gland-derived EpH4 cells, stably expressing either GFP-tagged podocalyxin or YFP-tagged E-cadherin, were subjected to hypo-osmotic stress (Fig. 1 E). As in MDCK II cells, the fluorescence intensity of podocalyxin was constant despite the expansion of the apical membrane, indicating that the targeted delivery of apical membrane proteins during apical membrane expansion is a conserved strategy in epithelial cells (Fig. 1, F and G).

We previously showed that sphingomyelin is abundant in the apical membrane (Ikenouchi et al., 2012). Therefore, we examined whether the expansion of apical membrane by the hypo-osmotic stress changes the lipid composition of the apical membrane. When we probed the distribution of sphingomyelin in cells under hypo-osmotic stress by using Lysenin, a sphingomyelin-binding toxin derived from earthworms (Yamaji et al., 1998), we found that the amount of GFP-Lysenin bound to the apical membrane increased correspondingly with the apical membrane expansion, suggesting that hypoosmotic stimulation augments sphingomyelin at the apical membrane (Figs. 1, H and I).

Next, we examined changes in the subcellular localization of caveolin, which is involved in the expansion of plasma

membranes, induced by hypo-osmotic stress in the non-epithelial cells (Kozera et al., 2009). Cav-1 and Cav-2, two major isoforms of caveolin expressed in EpH4 cells, were localized at the basolateral membrane in EpH4 cells (Fig. S1, A and B). Furthermore, the subcellular localization of GFP-tagged Cav-2 was unchanged by the treatment with hypo-osmotic medium (Fig. S1, C and D). Therefore, it is unlikely that caveolae contribute to the expansion of the apical membrane after hypo-osmotic challenge in EpH4 cells. In MDCK II cells, Cav1 was localized at the apical membrane (Fig. S1 E). Hypo-osmotic stress actually caused a slight decrease in the amount of Cav1 at the plasma membrane, but the amount of membrane supply due to the decrease in Cav1 was considerably smaller than the expanded surface area of the apical membrane (Fig. S1, F and G). These observations suggest that there may be additional molecular mechanisms that regulate apical expansion induced by hypo-osmotic stress, besides the supply of membrane provided by disrupting caveolae.

Visualization of apical membrane transport vesicles containing sphingomyelin

Based on the above observations, we hypothesized that the expansion of the apical membrane after hypo-osmotic challenge is due to the increased transport of vesicles containing apical membrane components such as sphingomyelin. Therefore, we first sought to visualize the apical transport of sphingomyelin using Lysenin (Lys). We constructed an artificial probe named SS-GFP-Lys by fusing the preprotrypsin signal sequence peptide (MSALLLILALVGAAVAFPVD) and EGFP to non-toxic Lys. As controls, a construct lacking a secretion signal (GFP-Lys) and a construct incorporating a mutation into an amino acid essential for binding to sphingomyelin (SS-GFP Lys^{WA}) were prepared (Fig. 2, A and B; Kiyokawa et al., 2004). We expressed these constructs in EpH4 cells and established stable cell lines (Fig. 2 C). There was no significant difference in the ratio of sphingomyelin to total phospholipids between wild-type and SS-GFP-Lys cells, which lead us to conclude that the expression of the probe is unlikely to affect sphingomyelin metabolism (Fig. 2 D). SS-GFP-Lys co-localized with GM130, a Golgi-apparatus marker protein, whereas neither GFP-Lys nor SS-GFP Lys^{WA} did so (Fig. 2 E). We examined the co-localization of SS-GFP-Lys with other organelle marker proteins. The cytoplasmic dots of SS-GFP-Lys co-localized with trans-Golgi network protein (TGNP), another Golgi-apparatus marker protein, but not with other organelle markers, such as the endoplasmic reticulum marker protein (Sec61 β), the lysosomal marker protein (LAMP-1), endosomal marker proteins (Rab5 or Rab7A), or the mitochondrial marker protein (Mito-7; Fig. S2, A and B). These observations are consistent with the finding that the synthesis and accumulation of sphingomyelin occur in the lumen of the Golgi-apparatus (Futerman et al., 1990; Deng et al., 2016). Furthermore, when EpH4 cells stably expressing SS-GFP-Lys were treated with Myriocin, an inhibitor of sphingomyelin biosynthesis, or HPA-12, an inhibitor of ceramide transport, the fluorescence intensity of SS-GFP-Lys was attenuated in accordance with the reduced amount of sphingomyelin (Fig. 2, F and G). We quantified the fluorescence of cytoplasmic vesicles containing SS-GFP-Lys and

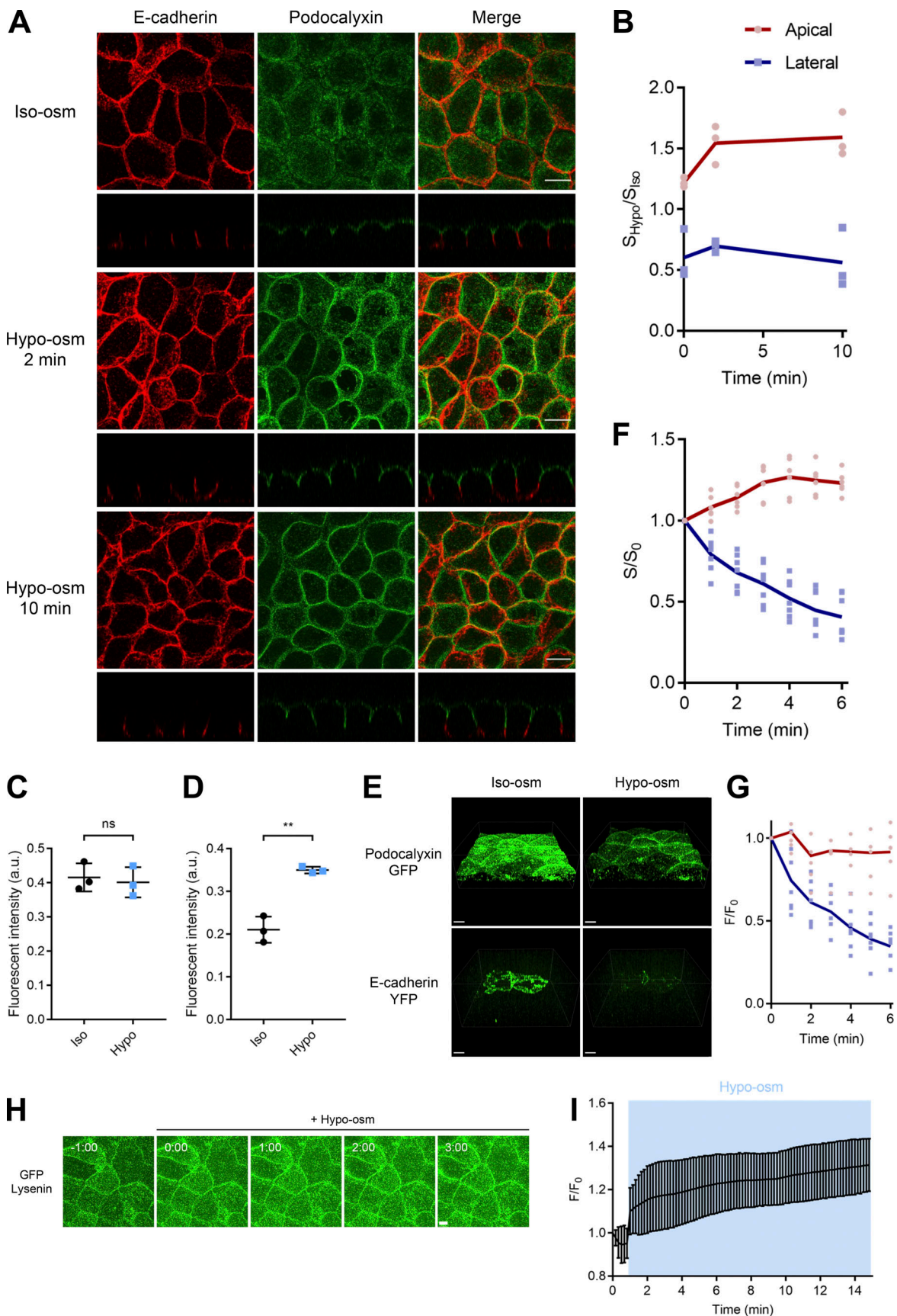


Figure 1. **Selective expansion of apical membrane of epithelial cells induced by hypo-osmotic stress.** (A) Wild-type MDCK cells were treated with hypo-osmotic buffer (150 mOsm/liter) for indicated times. Cells were stained with anti-GP135/podocalyxin mAb (green) and anti-E-cadherin mAb (red). Scale bar,

10 μm . **(B)** Quantification of the changes of apical plasma membrane area stained with anti-GP135/podocalyxin mAb (red line) and lateral plasma membrane area stained with anti-E-cadherin mAb (blue line). The ratio of surface area under hypo-osmotic stress (S_{Hypo}) to surface area under iso-osmotic stress (S_{Iso}) from $N = 3$ independent experiments were plotted. Surface rendering of the plasma membrane area (S) by each antibody staining was performed using Imaris 9.6 software (Bitplane, Inc.). **(C)** Quantification of E-cadherin fluorescence intensities in (A) under iso-osmotic and hypo-osmotic (2 min) conditions. $N = 3$ independent experiments; error bar, SD; ns, not significant by Student's t test. **(D)** Quantification of podocalyxin fluorescence in A under iso-osmotic and hypo-osmotic (2 min) conditions. $N = 3$ independent experiments; error bar, SD; **, $P = 0.0016$ by Student's t test. **(E)** EpH4 cells expressing GFP-tagged podocalyxin or YFP-tagged E-cadherin were treated with hypo-osmotic buffer (150 mOsm/liter) for 6 mins. Scale bar, 7 μm . **(F)** Quantification of the change of the surface area positive for GFP-tagged podocalyxin (red line) or YFP-tagged E-cadherin (blue line). The ratio of surface area at indicated time (S) to surface area at time point = 0 (S_0) were plotted from $N = 6$ independent experiments for GFP-tagged podocalyxin and $N = 7$ independent experiments for YFP-tagged E-cadherin. Surface rendering of the plasma membrane area (S) by each antibody staining was performed using Imaris 9.6 software (Bitplane, Inc.). **(G)** Time course change in the ratio of fluorescence intensity (F) under hypo-osmotic stress to fluorescence intensity at time point = 0 (F_0) of GFP-tagged podocalyxin (red line) or YFP-tagged E-cadherin (blue line) from data obtained with (Fig. 1 E). **(H)** Time-lapse imaging of EpH4 cells stained with purified GFP-Lysenin. Hypo-osmotic buffer (150 mOsm) containing the same concentration of purified GFP-Lysenin as in iso-osmotic medium was added at time 0:00. Scale bar, 5 μm . **(I)** Time course change in the fluorescence intensities of GFP-Lysenin normalized to the value at $t = 0$ min. Cells cultured in iso-osmotic medium were exposed to 150 mOsm medium at $t = 1$ min. Frames were taken every 10 s. Means with standard deviations from $N = 3$ independent experiments are shown.

confirmed that both inhibitors significantly decreased cytoplasmic SS-GFP-Lys-positive vesicles (Fig. 2 H). Based on the above results, we concluded that SS-GFP-Lys can be used as a probe to visualize the intracellular transport of sphingomyelin from the Golgi-apparatus to the plasma membrane.

Next, we examined whether specific proteins are incorporated into the sphingomyelin-containing vesicles that emerge from the trans-Golgi network (TGN). We established EpH4 cells expressing SS-GFP-Lys with either E-cadherin-mCherry as a marker for basolateral membrane transport or podocalyxin-like1 (PODXL1)-mScarlet as a marker for apical membrane transport (Fig. 3 A). We previously reported that podocalyxin-1 preferentially partitions into sphingomyelin-enriched membrane domains of the apical membrane in epithelial cells (Ikenouchi et al., 2013). Consistently, SS-GFP-Lys and PODXL1-mScarlet co-localized in cytoplasmic vesicles; GPI-mScarlet also co-localized with SS-GFP-Lys. In contrast, SS-GFP-Lys and E-cadherin-mCherry consistently localized in separate vesicles (Fig. 3 B). The fact that apical marker proteins specifically co-localized with SS-GFP-Lys in cytoplasmic vesicles supports the notion that sphingomyelin-rich transport vesicles are delivered to the apical membrane in polarized epithelial cells. We tested whether the vesicles containing SS-GFP-Lys were delivered to the apical membrane or the basolateral membrane by culturing the epithelial cells expressing SS-GFP-Lys in a two-chamber Transwell filter system and quantifying the amount of SS-GFP-Lys protein secreted into each chamber (Fig. 3 C). SS-GFP-Lys was released exclusively into the apical chamber, strongly suggesting that sphingomyelin-containing vesicles are selectively transported to the apical membrane (Fig. 3 D).

Inhibition of the mTORC2 pathway impairs apical transport of sphingomyelin

We next sought to elucidate the signaling pathways involved in the polarized transport of sphingomyelin by performing an inhibitor library screening (the Screening Committee of Anti-cancer Drugs [SCADS] Inhibitor kit III, containing 384 kinase inhibitors) to identify inhibitors that altered the subcellular distribution of SS-GFP-Lys. Among them, we identified Torin-1 and Ku0063794, which increased the number of SS-GFP-Lys-positive vesicles in the cytoplasm (Figs. 4 A and S2 C for low magnification images). We quantified SS-GFP-Lys fluorescence

in the cytoplasm to confirm that both the inhibitors significantly increased cytoplasmic SS-GFP-Lys vesicles (Fig. 4 B). Furthermore, co-localization between SS-GFP-Lys and Giantin significantly diminished under treatment with both inhibitors, indicating that the increased SS-GFP-Lys fluorescence reflects the cytoplasmic and not the unbudded, Golgi-tethered pool (Fig. 4 C). Interestingly, both are inhibitors of the mammalian target of rapamycin (mTOR) signal pathway. Therefore, we focused on the roles of mTOR signaling pathway in the following experiments.

To exclude the possibility that the effect observed by these mTOR inhibitors is due to the off-target effect and to narrow down which of the mTORC1 and mTORC2 pathways is responsible for the transport of sphingomyelin, we established EpH4 cells in which either Raptor or Rictor, essential scaffold proteins of mTORC1 or mTORC2 respectively, were knocked down (Liu and Sabatini, 2020; Fig. 4 D). The phosphorylation level of Akt Ser473 was significantly decreased in Rictor KD cells, as reported previously (Guertin et al., 2006; Fig. 4 D). In Rictor KD cells, but not in Raptor KD cells, the number of vesicles containing sphingomyelin in the cytoplasm increased significantly, as in the case of cells treated with mTOR inhibitors (Fig. 4, E-G). Therefore, we concluded that inhibition of the mTORC2 pathway increases intracellular transport vesicles containing sphingomyelin toward the apical membrane.

Why does mTORC2 inhibition increase sphingomyelin-containing in the cytoplasm? We hypothesized three possibilities: (1) inhibition of mTORC2 pathway up-regulated sphingomyelin biosynthesis; (2) inhibition of mTORC2 pathway enhanced budding of sphingomyelin-containing vesicles from the TGN; and (3) inhibition of mTORC2 pathway impaired the delivery of sphingomyelin containing vesicles to the apical membrane.

We first examined whether the biosynthesis of sphingomyelin increased under mTORC2 inhibition. We quantified the total amount of sphingomyelin in control wild-type EpH4 cells (WT), cells treated with mTORC inhibitors, and Rictor KD cells. Inhibition of mTORC2 pathway did not change the percentage of sphingomyelin in total phospholipids in whole cells, indicating that the biosynthesis of sphingomyelin was unaffected by mTORC2 inhibition (Fig. S3, A and B).

Next, we investigated whether inhibition of the mTORC2 pathway accelerates the formation of sphingomyelin-containing

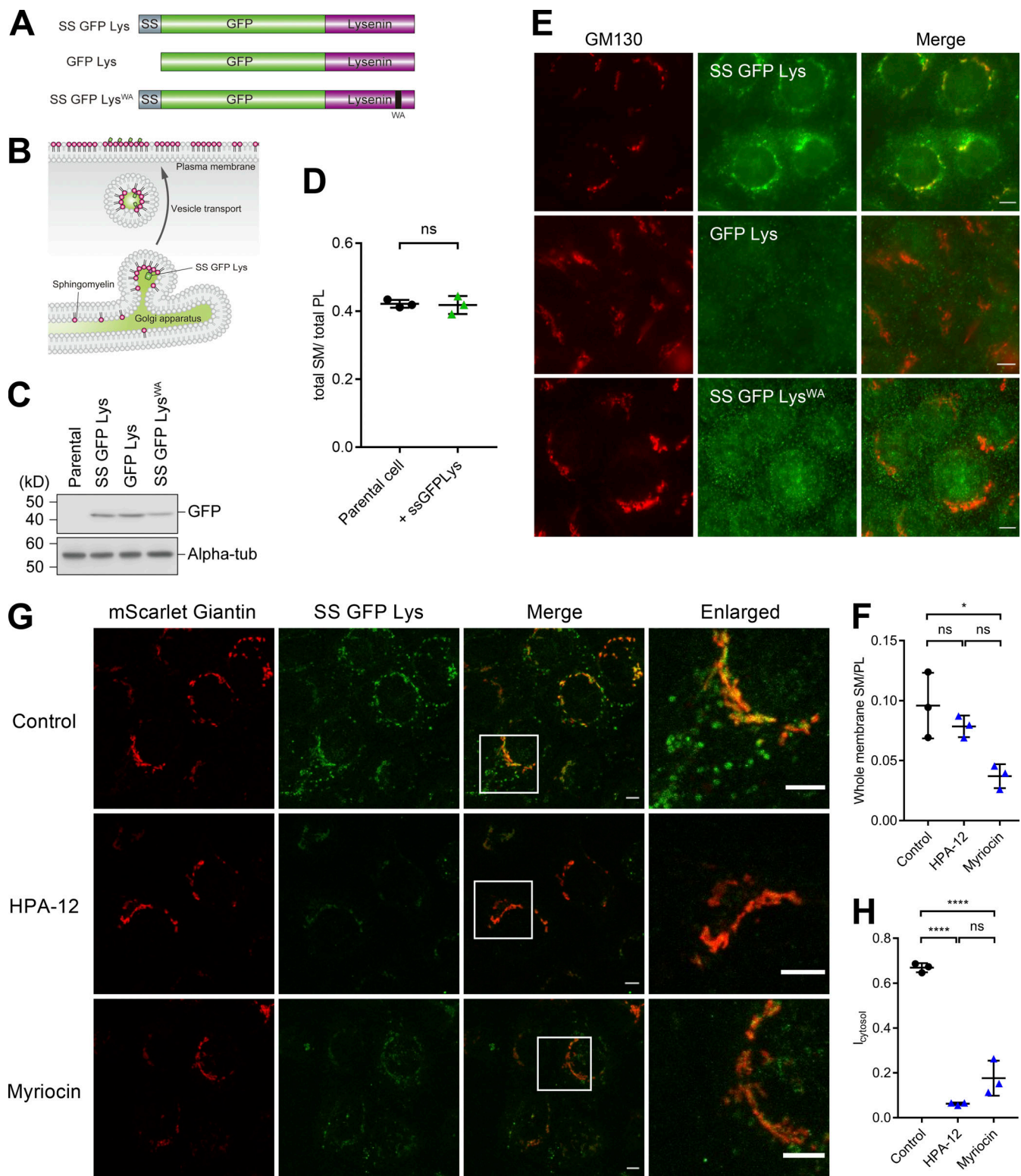


Figure 2. Visualization of transport vesicles to apical membrane containing sphingomyelin. (A) A schematic diagram of the construct to visualize intracellular trafficking of sphingomyelin. SS means the preprotrypsin signal peptide (MSALLILALVGA AVFPVD). (B) SS-GFP-Lys is expected to reside in the Golgi apparatus or the transport vesicles budding from TGN due to the binding to sphingomyelin synthesized and accumulated in the Golgi apparatus. When transport vesicles were fused with the plasma membrane, SS-GFP-Lys is released into the medium. (C) Total cell lysate of EpH4 cells stably expressing SS-GFP-Lys, GFP-Lys, and SS-GFP-Lys^{WA} were resolved by SDS-PAGE and immunoblotted with anti-GFP mAb and anti-alpha-tubulin mAb. (D) Total lipids were extracted from parental EpH4 cells and EpH4 cells expressing SS-GFP-Lys by Bligh and Dyer method. The ratio of the amount of sphingomyelin (mg/dl) to the total amount of phospholipids (mM) were plotted for both samples. *N* = 3 from independent experiments; error bar, SD; ns, not significant by Student's *t* test. (E) EpH4 cells stably expressing SS-GFP-Lys, GFP-Lys, and SS-GFP-Lys^{WA} were fixed and stained with anti-GM130 mAb (red). Only SS-GFP-Lys co-localized

with GM130. Scale bar, 10 μm . **(F)** EpH4 cells were treated with DMSO (control) or 40 μM HPA-12 or 50 μM Myriocin for 36 h. Then, total lipids were extracted by Bligh and Dyer method and the amount of total phospholipids (mM) and sphingomyelin (mg/dl) were quantified. $N = 3$ from independent experiments; error bar, SD; *, $P = 0.0162$; and ns, not significant by one-way ANOVA with Tukey's post-hoc test. **(G)** EpH4 cells stably expressing both SS-GFP-Lys and mScarlet-Giantin were treated with DMSO (control) or 40 μM HPA-12 or 50 μM Myriocin for 36 h. Scale bar, 5 μm . **(H)** The quantification of the cytoplasmic SS-GFP-Lys vesicles in cells treated with DMSO (control) or 40 μM HPA-12 or 50 μM Myriocin for 36 h. I_{cytosol} was calculated as (total area of SS-GFP-Lys – the area of SS-GFP-Lys that is colocalized with Giantin)/Total area of GFP. $N = 3$ from independent experiments; error bar, s.d.; ****, $P < 0.0001$; and ns, not significant by one-way ANOVA with Tukey's post-hoc test. Source data are available for this figure: SourceData F2.

vesicles from the TGN (Fig. S3). We first incubated WT cells or Rictor KD cells at 20°C for 2 h to block vesicle budding from the TGN, which resulted in the accumulation of SS-GFP-Lys in the Golgi apparatus and consequent depletion of SS-GFP-Lys in the cytoplasm. Importantly, the release of the 20°C-block by incubating the cells at 37°C for just 15 min induced the re-appearance of SS-GFP-Lys-containing vesicles in the cytoplasm. While the rate of vesicle formation did not significantly differ between WT and Rictor KD cells during the early phase of vesicle release from the TGN, there was a conspicuous accumulation of SS-GFP-Lys-positive vesicles over time only in the Rictor KD cells (Fig. S3 C). These observations strongly endorse the third possibility that the mTORC2 pathway regulates the delivery of sphingomyelin-containing vesicles to the apical membrane. We further tested this idea by enzymatically degrading sphingomyelin with bSMase and comparing its recovery at the apical membrane between WT and Rictor KD EpH4 cells. Sphingomyelin was visualized using the recombinant RFP-Lysenin protein (Fig. 5 A). Restoration of sphingomyelin at the apical membrane was observed from about 24 h after bSMase treatment in WT cells but not until around 72 h in Rictor KD cells, indicating that the delivery of sphingomyelin-containing vesicles to the apical membrane requires mTORC2 activity (Fig. 5 B).

Suppression of mTORC2 pathway reduces the amount of sphingomyelin in the apical membrane and impairs microvilli formation

Since the supply of sphingomyelin to the apical membrane is reduced in Rictor KD cells, we examined whether the amount of sphingomyelin in the apical membrane is constantly lower in Rictor KD cells as compared to WT cells. We isolated the apical membrane from both the cells by utilizing the nitrocellulose membrane method (Gerl et al., 2012). As expected, the amount of sphingomyelin in the apical membrane was significantly decreased in Rictor KD cells as compared to WT cells (Fig. 5 C). As sphingomyelin is enriched in the transport vesicles containing podocalyxin family proteins (Fig. 3 A), we examined whether the apical transport of podocalyxin was also impaired by the inhibition of mTORC2 pathway. As expected, podocalyxin failed to accumulate at the apical membrane in cells treated with Torin-1 (Fig. 5 D).

We previously reported that the removal of sphingomyelin from the apical membrane by treatment with bSMase causes the elimination of microvilli (Ikenouchi et al., 2013). Therefore, we examined whether microvilli formation is impaired in Rictor KD cells by scanning electron microscopy (SEM; Fig. 5 E). Indeed, microvilli were absent from the apical surface of Rictor KD cells to a degree similar to cells treated with bSMase, indicating that the amount of sphingomyelin transported to the apical

membrane in Rictor KD cells is insufficient to support microvilli formation. Taken together, we concluded that the activation of mTORC2 pathway plays essential roles in microvilli formation by promoting the intracellular transport of sphingomyelin to the apical membrane.

mTORC2 plays essential roles in the epithelial cyst formation by promoting apical transport of vesicles containing sphingomyelin and podocalyxin

Considering that sphingomyelin co-localizes with podocalyxin at the apical membrane (Ikenouchi et al., 2013) and that SS-GFP-Lys localizes in vesicles containing podocalyxin at a very high rate (Fig. 3 B), it appears that mTORC2 controls the polarized transport of vesicles containing apical membrane components. To examine the generality of this mechanism, we investigated the involvement of the mTORC2 pathway in the epithelial cyst formation of MDCK II cells. Podocalyxin plays an important role in both epithelial lumen and vascular endothelial lumen formation (Meder et al., 2005; Strlič et al., 2009). During the early phase of epithelial cyst formation, single MDCK II cells or doublets have inverted polarity such that podocalyxin is found at the ECM-abutting surface but excluded from cell-cell contacts. Integrin-mediated ECM sensing induces endocytosis of podocalyxin and transcytosis to the apical membrane initiation site (AMIS), a zone at the cell-cell contact of doublets (Bryant et al., 2014). As inhibition of the mTORC2 pathway impairs the transport of vesicles containing sphingomyelin and podocalyxin to the apical membrane in the two-dimensional culture of EpH4 cells (Fig. 5, A and D), we tested whether mTORC2 inhibition or reduction of sphingomyelin impairs transcytosis of podocalyxin to the apical membrane in three-dimensional MDCK II cysts (Fig. S4 A). Treatment with either HPA-12, an inhibitor of sphingomyelin biosynthesis, or Torin-1, an mTOR inhibitor, impaired the apical transport of podocalyxin and led to abnormal multi-lumen formation (Fig. S4, A and B). Based on these results, we concluded that the regulation of sphingomyelin transport to the apical membrane by mTORC2 is important for the formation of the epithelial lumen.

Then, how does the loss of mTORC2 activity impair the apical transport of sphingomyelin-containing vesicles? We noted that the phenotype of cyst formation in MDCK II cells treated with mTOR inhibitors was similar to those in which Rab35 activity is down-regulated (Klinkert et al., 2016; Mrozowska and Fukuda, 2016). Furthermore, Rab35 is reported to interact directly with the cytoplasmic region of podocalyxin and tether the transport vesicles containing podocalyxin to the apical membrane (Klinkert et al., 2016; Mrozowska and Fukuda, 2016). Therefore, we next examined whether Rab35 functions as an effector of the mTORC2 pathway in the regulation of apical transport of

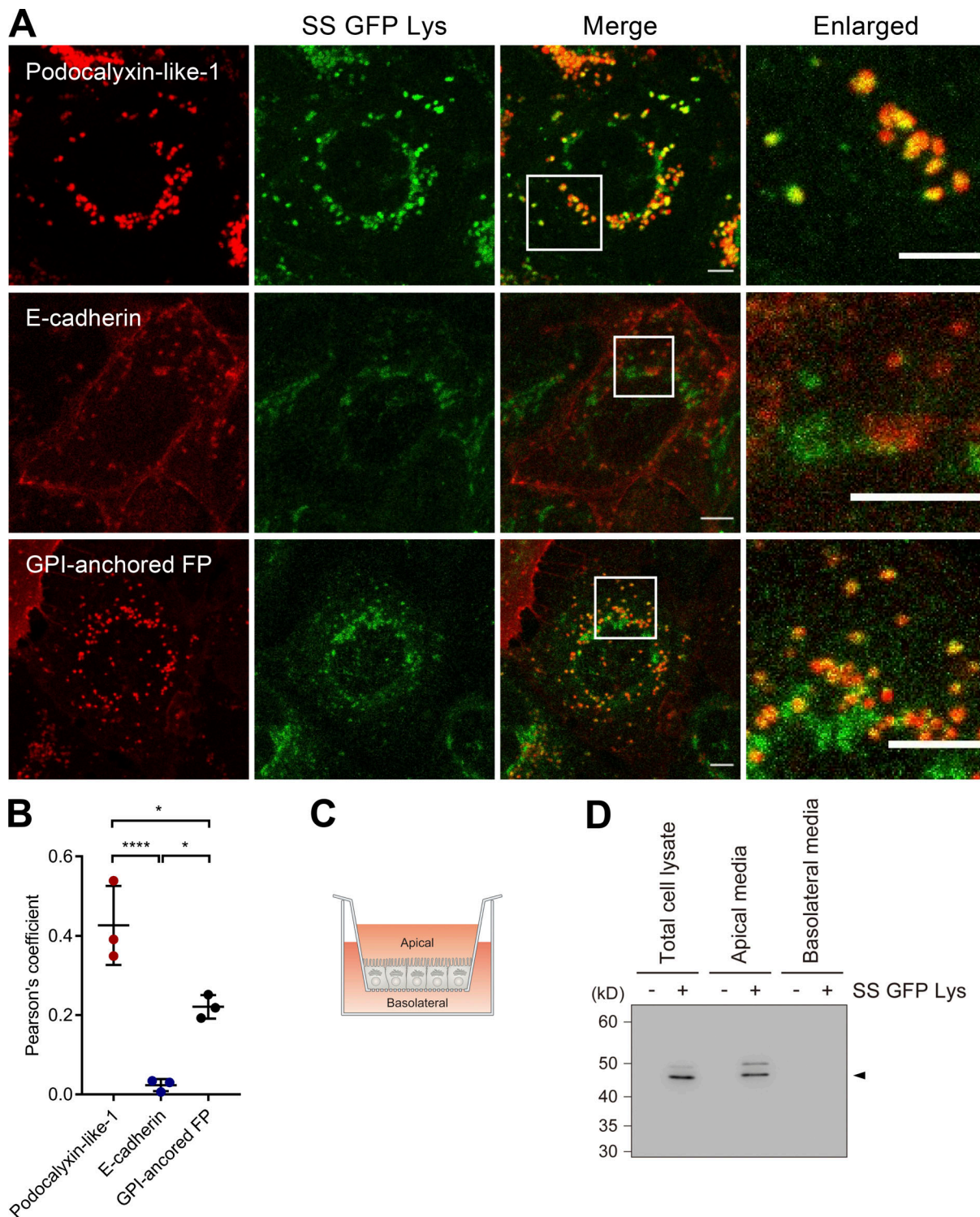


Figure 3. SS-GFP-Lys is transported together with podocalyxin to the apical membrane. (A) EpH4 cells stably expressing SS-GFP-Lys were transfected with one of GPI-mScarlet, E-cadherin-mCherry, or Podocalyxin-like-1-mScarlet (PODXL1-mScarlet). Living cells were observed with a confocal microscope at 37°C. GPI-mScarlet and PODXL1-mScarlet showed co-localization with SS-GFP-Lys dots, but E-cadherin-mCherry did not. Scale bar, 5 μ m. (B) The degree of co-localization between SS-GFP-Lys and one of GPI-mScarlet, E-cadherin-mCherry, or PODXL1-mScarlet was analyzed by Pearson's correlation coefficient in colocalization (ImageJ). $N = 3$ independent experiments; error bar, SD; ****, $P = 0.0005$; *, $P(\text{Podocalyxin-like-1}) = 0.0143$; and *, $P(\text{E-cadherin}) = 0.0170$ by one-way ANOVA with Tukey's post-hoc test. (C) EpH4 cells stably expressing SS-GFP-Lys were cultured on a two-chamber filter and grown to confluence. After 48 h of culture, the medium of the apical side and that of the basolateral side were collected and concentrated 30-fold. (D) Samples obtained as in Fig. 3 C were resolved by SDS-PAGE and immunoblotted with anti-GFP mAb. Arrowhead indicates the expected molecular weight of SS-GFP-Lys. Source data are available for this figure: SourceData F3.

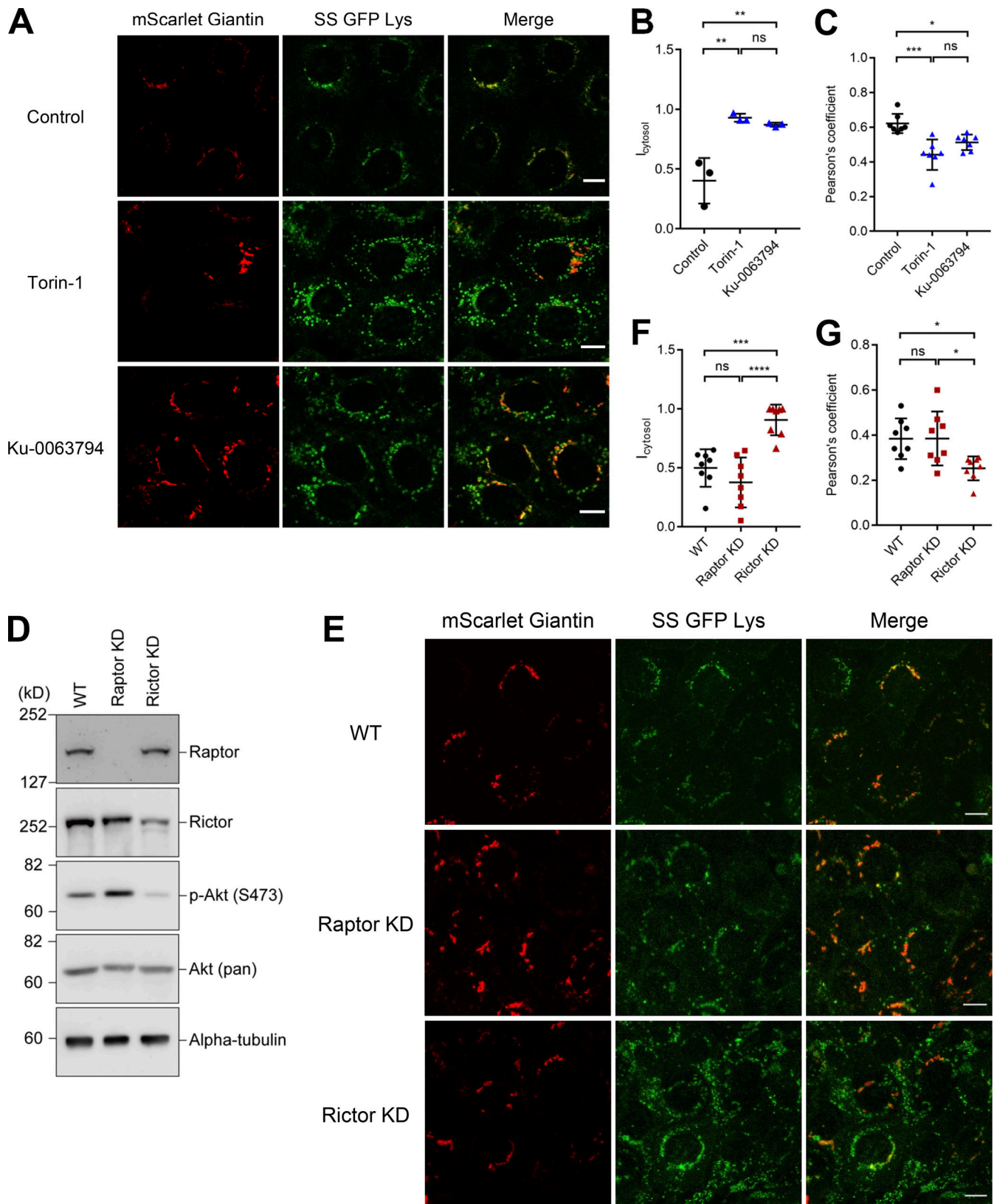


Figure 4. **Inhibition of the mTORC2 pathway impairs apical transport of sphingomyelin.** (A) EpH4 cells stably expressing SS-GFP-Lys and mScarlet-Giantin were treated with DMSO (Control), 250 nM Torin-1, or 3 μ M Ku-0063794 for 12 h. Treatment with mTOR inhibitors increases the dot-like cytoplasmic SS-GFP-Lys vesicles without changing morphology of the Golgi apparatus. Scale bar, 10 μ m. (B) Quantification of the cytoplasmic SS-GFP-Lys vesicles in cells treated with DMSO (Control), 250 nM Torin-1 or 3 μ M Ku-0063794 for 24 h. $N = 3$ independent experiments; error bar, SD; **, $P(\text{Torin-1}) = 0.0029$; **, $P(\text{Ku-0063794}) = 0.0052$; and ns, not significant by one-way ANOVA with Tukey's post-hoc test. (C) Quantification of Pearson's correlation coefficient between

SS-GFP-Lys and Giantin in cells treated with DMSO (Control), 250 nM Torin-1, or 3 μ M Ku-0063794 for 12 h. $N = 7$ from independent experiments; error bar, SD; ***, $P = 0.0002$; *, $P = 0.0157$; and ns, not significant by one-way ANOVA with Tukey's post-hoc test. **(D)** Total cell lysates of wild-type Eph4 cells (WT), Raptor knockdown (KD) and Rictor KD Eph4 cells were resolved by SDS-PAGE and immunoblotted with indicated antibodies. In Rictor KD cells, the level of Akt (Ser 473) phosphorylation are reduced as compared to wild-type Eph4 cells as described previously (Guertin et al., 2006). **(E)** Raptor or Rictor was knocked down in Eph4 cells stably expressing SS-GFP-Lys and mScarlet-Giantin. The cytoplasmic dots of SS-GFP-Lys were significantly increased in Rictor KD cells. Scale bar, 10 μ m. **(F)** Quantification of the cytoplasmic SS-GFP-Lys vesicles in WT cells, Raptor KD cells and Rictor KD cells. ($N = 8$ from independent experiments; error bar, SD, one-way ANOVA; ***, $P = 0.0003$; ****, $P < 0.0001$). **(G)** Quantification of Pearson's correlation coefficient between SS-GFP-Lys and Giantin in WT cells, Raptor KD cells and Rictor KD cells. $N = 8$ independent experiments; error bar, SD; *, $P(\text{WT}) = 0.0243$; *, $P(\text{Raptor KD}) = 0.0232$; and ns, not significant by one-way ANOVA with Tukey's post-hoc test. Source data are available for this figure: SourceData F4.

vesicles containing sphingomyelin and podocalyxin. Intriguingly, the expression of the dominant active form of Rab35 (Rab35-Q67L) enhanced the delivery of sphingomyelin-containing vesicles to the apical membrane, even in cells treated with mTOR inhibitors, as the SS-GFP-Lys-positive vesicles disappeared in cells expressing mScarlet-Rab35-Q67L, but not in cells expressing mScarlet only (Fig. 5 F). Moreover, cells expressing mScarlet-Rab35-Q67L were insensitive to Torin-1 treatment and exhibited normal podocalyxin transport to the apical membrane (Fig. S4 C). Thus, the activation of Rab35 can overcome the apical transport block induced by mTORC2 inhibition. Although the detailed molecular link between mTORC2 and Rab35 activation is unclear, these findings suggest that Rab35 is activated downstream of the mTORC2 pathway. Therefore, we further examined the functional relationship between the mTORC2-Rab35 axis and apical transport.

mTORC2-Rab35 axis promotes apical transport of sphingomyelin by reducing the actin cortex

To confirm that active Rab35 promotes apical transport of sphingomyelin, we examined whether expression of the dominant active form of Rab35 could restore sphingomyelin level at the apical membrane in Rictor KD cells after bSMase treatment (Fig. 6, A and B). GFP-Lysenin staining was observed 24 h after treatment with bSMase in Rictor KD cells expressing mScarlet-Rab35-Q67L, similar to WT cells, but not in cells expressing mScarlet only, indicating that expression of dominant active Rab35 up-regulates the recovery of sphingomyelin level at the apical membrane.

Next, we established cells in which Rab35 was knocked out to examine whether Rab35 is essential for the transport of sphingomyelin to the apical membrane (Fig. S5, A and B). In Rab35 KO cells, the number of vesicles containing sphingomyelin in the cytoplasm increased (Fig. S5 C). Apical transport of podocalyxin-1 was also impaired (Fig. S5 D). Restoration of sphingomyelin at the apical membrane after bSMase treatment was significantly delayed in Rab35 KO cells, indicating that the delivery of sphingomyelin-containing vesicles to the apical membrane requires Rab35 (Fig. S5, E and F). Furthermore, the formation of microvilli was severely diminished in Rab35 KO cells, which strongly supports the notion that Rab35 is required for the apical transport of sphingomyelin (Fig. S5 G).

Then, how does the mTORC2-Rab35 axis promote the apical transport of sphingomyelin? When we carefully observed Rictor KD cells, we found that the amount of actin cortex at the apical membrane was significantly increased compared with WT cells (Fig. 6, C and D). Notably, the expression of Rab35-Q67L

significantly reversed the accumulation of the actin cortex in the apical membrane of Rictor KD cells (Fig. 6, E and F). The actin cortex is known to function as a barrier that prevents the delivery and fusion of transport vesicles to the plasma membrane. Therefore, we reasoned that mTORC2-Rab35 pathway facilitates apical transport by decreasing the amount of the actin cortex.

Roles of mTORC2-Rab35 axis in the hypotonic stress response

Finally, we examined the functional importance of mTORC2-Rab35 axis in the expansion of the apical membrane as an adaptation to hypo-osmotic stress. First, we found that hypo-osmotic stress steadily increased the phosphorylation level of Akt at S473, an indicator of mTORC2 activation (Fig. 7, A and B). The increase in Akt phosphorylation was canceled by Torin-1 treatment, indicating that mTORC2 is activated by hypo-osmotic stress (Fig. 7, C and D). We also confirmed that the hypo-osmotic condition of this study does not activate apoptosis, as assessed by examining caspase activation using FlipGFP (Fig. 7, E and F).

Having established that hypo-osmotic stress activates mTORC2, we examined if the mTORC2-Rab35 axis is involved in the adaptation to hypo-osmotic stress. Exposure to a hypo-osmotic medium caused a significantly higher rate of cell death by rupturing the Rictor KD and Rab35 KO cells compared with WT cells (Fig. 7, G-I). Importantly, the over-expression of Rab35-Q67L suppressed cell death of Rictor KD cells exposed to hypo-osmotic medium, suggesting that Rab35 activation downstream of mTORC2 is essential for the adaptation to hypo-osmotic stress (Fig. 7 J, Video 1, and Video 2). Therefore, we tested whether Rab35 is activated in response to hypo-osmotic stress.

The F-actin monooxygenase molecule interacting with CasL protein (MICAL) is a Rab35 effector with a well-characterized Rab binding domain (RBD) that binds to GTP-bound Rab35 (Fukuda et al., 2008). The FLAG-tagged RBD of MICAL-3 (1,826-1,993 aa) was expressed in HEK293 cells and used to pull down active Rab35 from Eph4 cells stably expressing either WT Rab35 or Rab35-Q67L. Treatment with the hypo-osmotic medium increased the amount of active Rab35, which was suppressed in cells pre-treated with the mTOR inhibitors (Fig. 7, K and L). When expressed in WT cells, the GFP-tagged RBD of MICAL-3 was predominantly localized at the apical membrane, but treatment with Torin-1 significantly impaired its localization (Fig. 7, M and N). While the RBD of MICAL-3 protein has been shown to bind to the closely related Rab1 and Rab8 in addition to Rab35 (Rai et al., 2016), our biochemical and localization data considered together reasonably support the notion that mTORC2

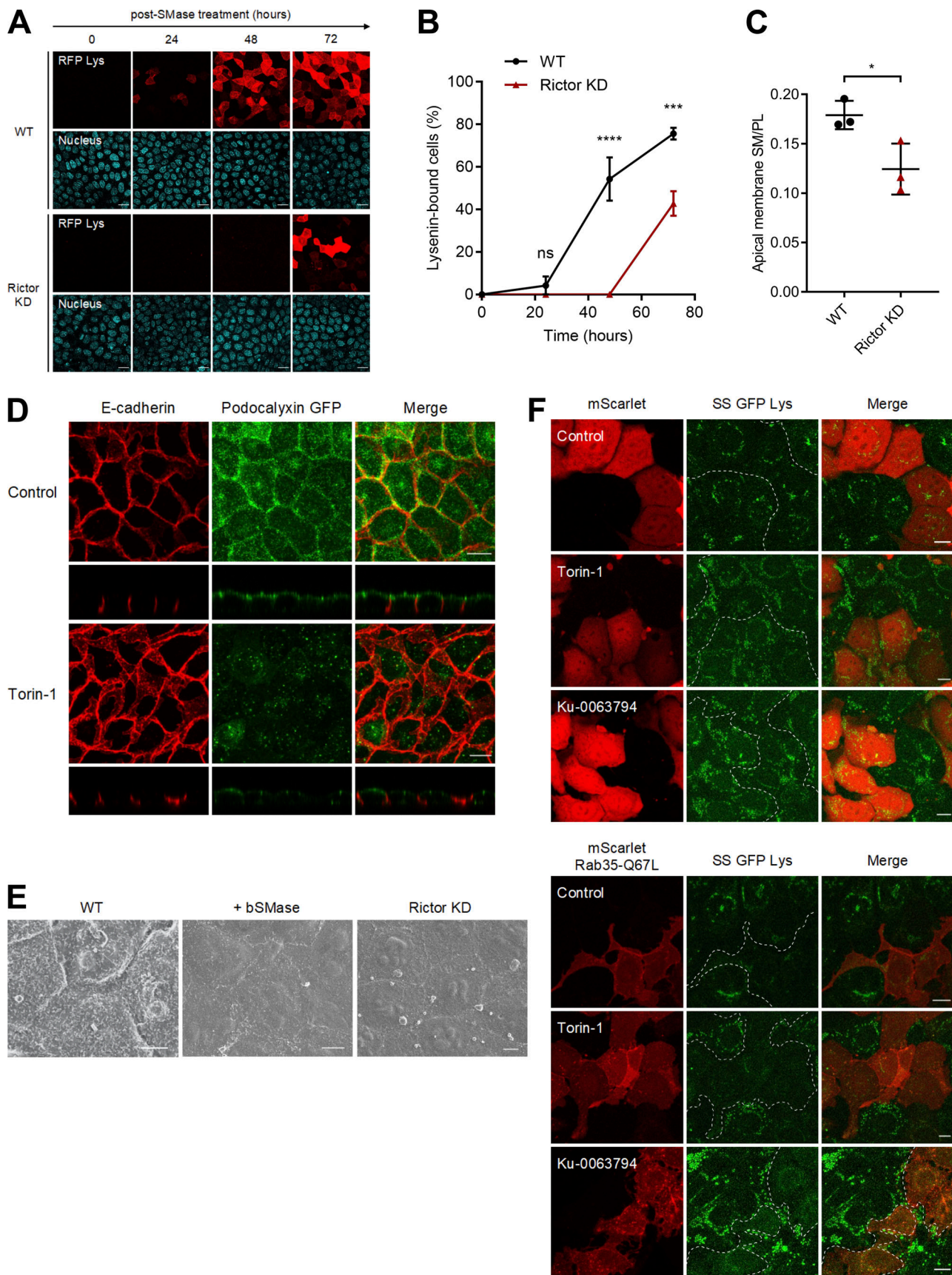


Figure 5. **Suppression of mTORC2 pathway reduces the amount of sphingomyelin in the apical membrane and impairs microvilli formation.** (A) Wild type Eph4 cells and Rictor KD cells were treated with bSMase to degrade sphingomyelin at the apical membrane. Then, bSMase was washed out and cultured

in a normal medium, and the recovery rate of sphingomyelin to the apical membrane of each cell was evaluated by the number of cells to which His-RFP-Lysenin binds. Scale bar, 20 μm . **(B)** The time-course change of number of cells stained with His-RFP-Lysenin after washing out bSMase in wild-type EpH4 cells and Rictor KD cells. $N \geq 3$ independent experiments; error bar, SD; ****, $P < 0.0001$; ***, $P < 0.0003$; and ns, not significant by Student's t test. **(C)** The apical membrane fractions of wild-type EpH4 cells and Rictor KD cells were isolated and the amount of sphingomyelin (mg/dl)/total phospholipid (mM) were quantified. $N = 3$ independent experiments; error bar, SD; *, $P = 0.0327$ by Student's t test. **(D)** Wild-type EpH4 cells stably expressing podocalyxin-GFP were treated with either DMSO (control) or 250 nM Torin-1 for 24 h. Cells were stained with anti-GFP mAb and anti-E-cadherin mAb. Scale bar, 10 μm . **(E)** Scanning electron microscopy of wild-type EpH4 cells, bSMase treated wild-type EpH4 cells and Rictor KD cells. Scale bar, 5 μm . **(F)** EpH4 cells stably expressing SS-GFP-Lys were transfected with either mScarlet only or mScarlet-tagged-Rab35 dominant active mutant (Q67L) expression vectors and treated with DMSO (Control), 250 nM Torin-1 or 3 μM Ku-0063794 for 24 h. Transfected cells are indicated by the white-dotted line. Scale bar, 10 μm .

activation is necessary to maintain a pool of active Rab35 at the apical membrane. Altogether, we conclude that mTORC2 regulates epithelial cell adaptation to hypo-osmotic stress by activating Rab35 to promote vesicle transport to the apical membrane.

However, it is still unclear how the mTORC2-Rab35 axis actually exerts its protective effect, particularly with regard to the apical actin cortex. We found that treatment with hypo-osmotic medium significantly reduced the actin cortex of the apical membrane while hardly altering that of the basolateral membrane (Fig. 8, A and B, see the cross-sections and Fig. 8 A and Video 3). Intriguingly, this was accompanied by a rapid decrease of PI(4,5)P2 at the apical membrane (Fig. 8, C and D; and Video 4); this was suppressed by treatment with Torin-1 (Video 1 and Video 2), suggesting that mTORC2 is involved in PI(4,5)P2 turnover (Fig. 8 D).

PI(4,5)P2 is enriched in the apical membrane of epithelial cells (Martin-Belmonte et al., 2007) and is an important regulator of actin assembly by mediating the anchorage of the actin network to the plasma membrane through linker proteins, such as ezrin/radixin/moesin (ERM) family proteins (Janmey et al., 2018). Additionally, the inositol polyphosphate 5-phosphatase OCRL-1 (also known as Lowe oculocerebrorenal syndrome protein) is a Rab35 effector molecule (Dambournet et al., 2011). Therefore, reduction of PI(4,5)P2 may be the downstream event in the mTORC2-Rab35 pathway that induces the reduction of the actin cortex at the apical membrane to facilitate vesicle tethering. To test this possibility, we examined whether forced reduction of PI(4,5)P2 is sufficient to enable the adaptive response to hypo-osmotic stress. When we expressed a chimeric construct, Src-INPP5E-Scarlet, in which the lipid modification motif of c-Src was fused to the catalytic domain of inositol polyphosphate-5-phosphatase E (INPP5E), the SS-GFP-Lys-positive vesicles that accumulated in the cytoplasm disappeared from Torin-1-treated cells (Fig. 8 E). Furthermore, the expression of Src-INPP5E-GFP suppressed cell rupture of Rictor KD cells caused by hypo-osmotic stress, suggesting that the reduction of PI(4,5)P2 is an essential adaptive response to hypo-osmotic stress initiated by mTORC2 (Fig. 8, F and G). Rab35 is also known to bind to and activate the redox enzyme MICAL family proteins and F-actin disassembly factors (Frémont et al., 2017). Therefore, it is possible that the oxidation-mediated depolymerization of actin filaments by MICAL family proteins is involved in the rapid reduction of the actin cortex at the apical membrane by hypo-osmotic stress. Thus, we propose that Rab35 initiates a two-pronged approach to reduce cortical actin at the apical membrane and thereby promote the transport of vesicles

containing apical membrane components, one through OCRL-1 to decrease the amount of PI(4,5)P2 and destabilize the plasma membrane-actin tether, and the other through the MICAL family proteins to locally disassemble F-actin (Fig. 8 H).

Taken together, mTORC2-Rab35 activation by hypo-osmotic stress not only promotes apical transport of sphingomyelin to the supply membrane but also decreases the actin cortex underlying the apical membrane by reducing PI(4,5)P2 to facilitate the expansion of the apical membrane (Fig. 8 H).

Discussion

Our understanding of how apical membrane components such as sphingomyelin are transported is limited. In this study, we showed that mTORC2 regulates the transport of sphingomyelin to the apical membrane possibly through the activation of Rab35. Furthermore, we clarified that the promotion of apically-targeted post-Golgi vesicle transport by activation of mTORC2-Rab35 is essential to prevent plasma membrane rupture in the hypotonic stress response of epithelial cells. Thus, we revealed that the maintenance of homeostasis of the apical membrane of epithelial cells is a previously uncharacterized function of mTORC2.

These conclusions are in good agreement with previously reported phenotypes in mice deficient for key components of mTORC2 signaling. For example, it was reported that one of the microvillar transporter, Na^+/H^+ exchanger 3 (NHE3), was mislocalized to the cytoplasm in small intestinal epithelial cells of mTOR conditional KO mice, which led to the dysfunction of microvilli and severe diarrhea (Yang et al., 2015). In addition, the phenotypes of conditional KO mouse of Raptor (Rap Δ Tubule), Rictor (Ric Δ Tubule), and both Raptor/Rictor (RapRic Δ Tubule) in the proximal tubule epithelial cells were also related to the dysfunction of apical membranes (Grahammer et al., 2017). In these KO mice, the morphology of microvilli in tubular epithelial cells was abnormal. In RapRic Δ Tubule mice, the amount of glucose and phosphate lost in urine increased 3.3-fold and 5-fold over the wild type, respectively, indicating that the resorption of the nutrients from urine was impaired. Although the reduction in both length and number of microvilli was observed in all of Rap Δ Tubule, Ric Δ Tubule, and RapRic Δ Tubule mice, RapRic Δ Tubule mice showed the most severe phenotype, suggesting that both mTORC1/mTORC2 signaling pathways are likely to contribute to the formation of microvilli additively, as more pronounced microvilli abnormalities were observed in double knockout mice compared to their respective single knockout mice. These

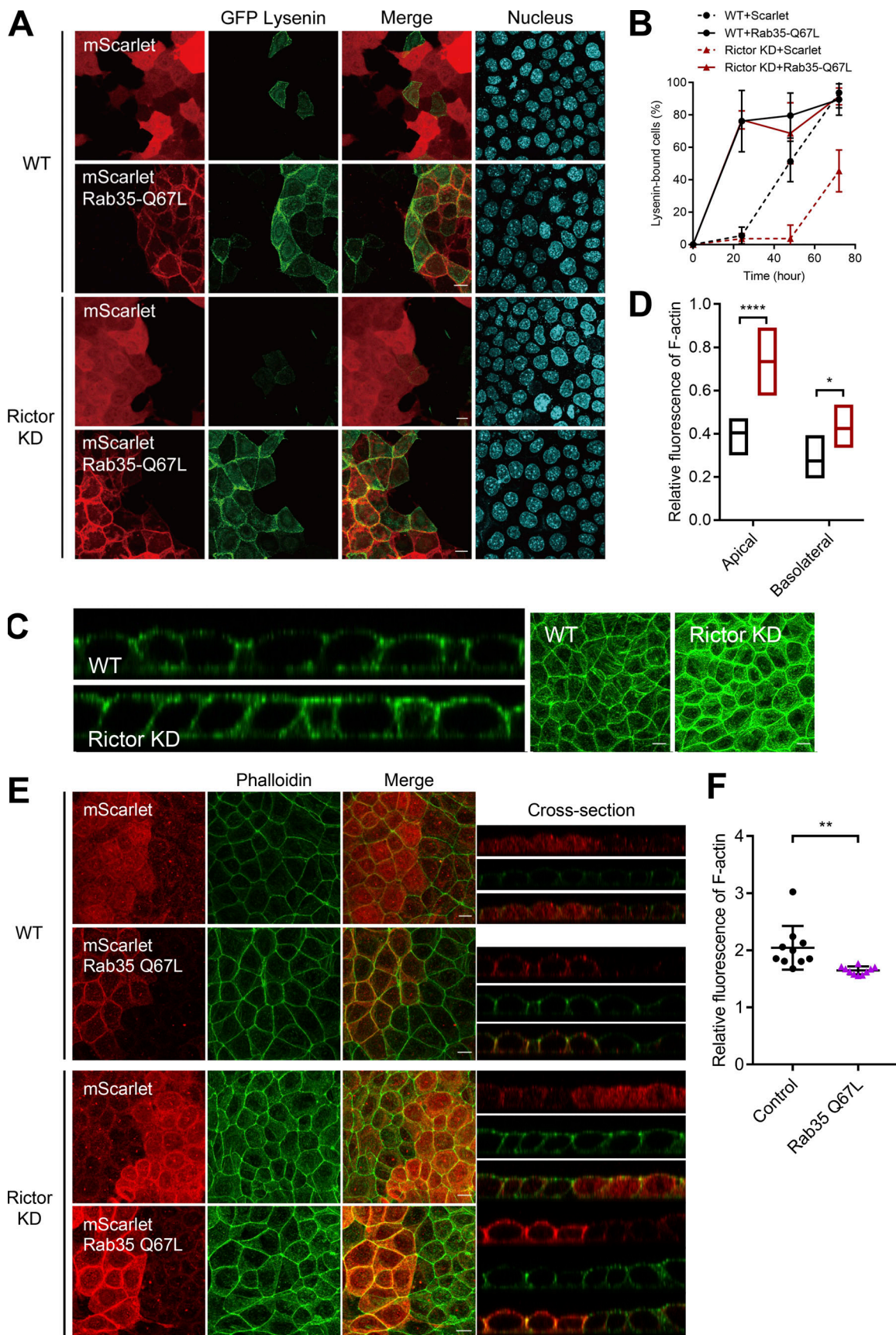


Figure 6. **Activation of Rab35 promotes apical transport of sphingomyelin via reduction of actin cortex of apical membrane.** (A) EpH4 wild-type (WT) cells and Rictor KD cells stably expressing either mScarlet only or mScarlet-tagged-Rab35 Q67L were treated with bSMase. bSMase was washed out and cells

were cultured in normal medium for an additional 24 h. Recovery of sphingomyelin at the apical membrane was imaged by recombinant GFP-Lysenin. Scale bar, 10 μ m. **(B)** Time course change in the number of GFP-Lysenin-positive cells at the apical membrane was quantified. $N \geq 3$ independent experiments; error bar, SD. **(C)** EpH4 wild-type (WT) cells and Rictor KD cells were stained with phalloidin. Scale bar, 10 μ m. **(D)** Quantification of the fluorescent intensity of phalloidin at the apical and basolateral membrane in wild-type EpH4 cells (black) and Rictor KD cells (red). $N = 5$ from independent experiments; error bar, SD, two-way ANOVA; *, $P = 0.0476$; ****, $P < 0.0001$. **(E)** EpH4 wild-type (WT) cells and Rictor KD cells stably expressing either mScarlet only or mScarlet-Rab35 Q67L were stained with phalloidin. Scale bar, 10 μ m. **(F)** Quantification of the fluorescence intensities of phalloidin at the apical membrane in mScarlet only expressing Rictor KD cells and mScarlet-Rab35 Q67L expressing Rictor KD cells. $N = 10$ independent experiments; error bar, SD; **, $P = 0.0048$ by Student's *t*-test.

studies on knockout mice clearly indicate the necessity of mTOR signaling in the formation of apical membrane structures; however, the underlying mechanisms remained unclear. In light of our finding, it is important to investigate whether apical transport of sphingomyelin is affected in the epithelial tissues of these knockout mice in future studies.

We revealed that activation of the mTORC2–Rab35 pathway by hypo-osmotic stress promotes the apical transport of sphingomyelin and enables rapid expansion of the apical membrane. Notably, in mTORC2 (Rictor) KD or Rab35 knockout cell lines, the formation of apical membrane structures such as microvilli was impaired and the transport of sphingomyelin apical membrane was delayed, suggesting that sustained activity of the mTORC2–Rab35 pathway is required to maintain epithelial cell morphology and function even in steady-state epithelial cells. Furthermore, under iso-osmotic condition, RBD of MICAL-3, a reporter of activated Rab35, constitutively localizes to the apical membrane, and its localization is impaired by pharmacological inhibition of the mTORC2 pathway, suggesting a constitutive role for the mTORC2–Rab35 axis at the apical membrane of polarized epithelial cells (Fig. 7 M). Therefore, in addition to the molecular mechanism by which hypo-osmotic stress induces further activation of the mTORC2–Rab35 pathway, elucidation of the upstream signaling pathway responsible for the constitutive activity of mTORC2–Rab35 in polarized epithelial cells is a topic of immediate interest.

In this study, we found that mTORC2 regulates the apical transport of sphingomyelin in mammalian cells. Curiously, in *Saccharomyces cerevisiae*, the activation of TORC2 regulates sphingolipid biosynthesis. In yeast, TORC2 is activated by various stresses in the plasma membrane, such as increased membrane tension. TORC2 was reported to up-regulate sphingolipid biosynthesis by several pathways. TORC2 activates Ypk1 and Ypk2 kinases, which are homologs of Akt and the human serum glucocorticoid-induced kinase SGK, respectively. Ypk1 acts downstream of TORC2 to phosphorylate Orm1/Orm2 and antagonize their activity as negative regulators of sphingolipid synthesis (Berchtold et al., 2012; Niles et al., 2012; Roelants et al., 2011). In addition, Ypk1 positively regulates the synthesis of ceramides, precursors of complex sphingolipids, by phosphorylating ceramide synthase (Muir et al., 2014). In yeast, Slm1 and its redundant paralog Slm2 were identified as upstream components of the TORC2–Ypk1 pathway. When the plasma membrane tension is increased by hypotonic shock, Slm1/2 is recruited to the plasma membrane region containing TORC2 (Berchtold and Walther, 2009), and it potentially activates TORC2–Ypk1 signaling by recruiting Ypk1 to TORC2 for activation (Berchtold et al., 2012). The activation of TORC2–Ypk1 leads to the increased production of sphingolipids, which reduces

plasma membrane tension (Riggi et al., 2018). Therefore, one of the important roles of TORC2–Ypk1 signaling pathway is to maintain plasma membrane tension homeostasis. On the other hand, our study revealed that mTORC2 regulates the vesicular transport of sphingomyelin to the apical membrane in mammalian epithelial cells without affecting sphingomyelin biosynthesis. Membrane stretch is reported to similarly induce mTORC2 signaling in mammalian cells (Diz-Muñoz et al., 2016), suggesting that TORC2 activation by increased plasma membrane tension is evolutionally conserved. Although the mammalian homolog of the membrane stress sensors Slm1 and Slm2 are not identified so far, it is necessary to investigate whether the sensing mechanisms of sphingomyelin levels at the plasma membrane and the regulatory mechanisms to maintain the homeostasis of sphingomyelin levels with by TORC2 activity are evolutionally conserved in future studies.

Materials and methods

Reagents

Eph4 cells were grown in DMEM supplemented with 10% FCS. The cDNA encoding Lysenin (161–298 aa) was amplified by PCR, supplemented with preprotrypsin signal peptide (MSALLI-LALVGA AVAFPVD) and GFP tag, and ligated into pCAGGS-Neo vector. Eph4 cells were transfected with expression vectors of SS-GFP-Lys, GFP-Lys, or SS-GFP-Lys^{WA} in OPTI-MEM (Thermo Fisher Scientific) using Lipofectamine 3000 (Thermo Fisher Scientific). After a 2-wk selection in growth medium containing G418, we established Eph4 cells stably expressing these vectors. Raptor KD and Rictor KD Eph4 cells were established by transfecting pLKO mouse shRNA 1 raptor (Plasmid#21339 from Addgene) and pLKO mouse shRNA 1 Rictor (Plasmid #21341 from Addgene) vectors, respectively. E-cadherin-mCherry expressing Eph4 cells were established by transfecting pLL5.0 E-cadherin shRNA/mE-cadherin-mCherry (Plasmid #101282 from Addgene). Human podocalyxin-like-1 (PODXL1) cDNA and Human MICAL-3 were amplified by PCR using the cDNA library of CaCO-2 cells as a template. The amplified fragment supplemented with mScarlet was sub-cloned into the pLenti CMV Neo DEST vector (Plasmid #17392 from Addgene). pmScarlet-H_Giantin_C1 (Plasmid #85049), Myc-Rab35 WT (Plasmid #47433), Myc-Rab35 Q67L (Plasmid #405909), and pcDNA3-FlipGFP (Casp3 cleavage seq) T2A mCherry (Plasmid #124428) were obtained from Addgene. For each construct, more than three independent clones were established and it was confirmed that all clones showed the same phenotypes.

His-RFP-Lysenin (161–298 aa) or His-GFP-Lysenin was expressed in *Escherichia coli* and purified by affinity chromatography

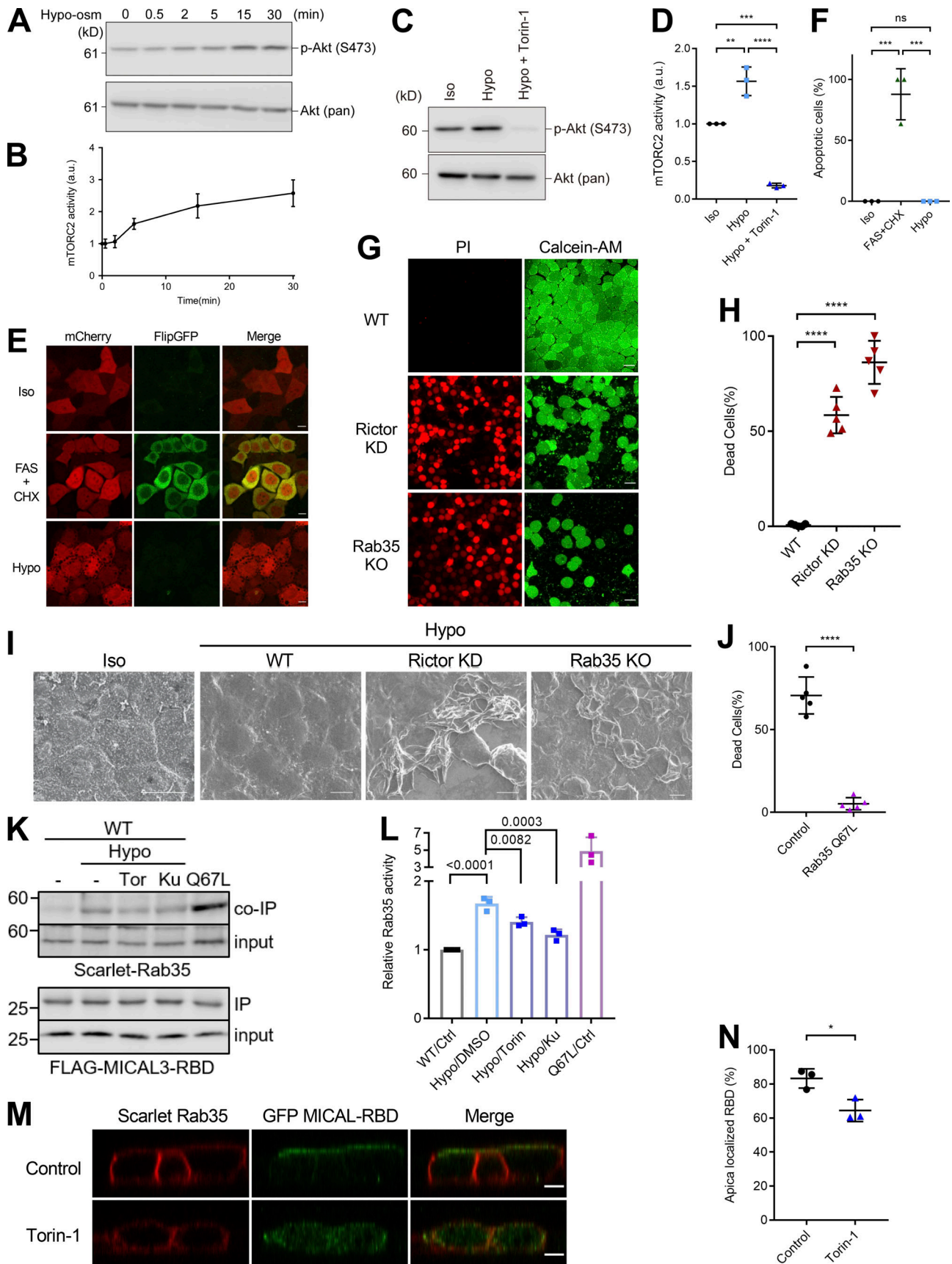


Figure 7. **mTORC2-Rab35 activity is required for the adaptation to increased apical plasma membrane tension under hypo-osmotic stress. (A and B)** mTORC2 activity under hypo-osmotic condition (150 mOsm/liter) were assessed by phosphorylation level of Akt Ser473 in EpH4 cells. *N* = 6 independent

experiments. **(C)** Total cell lysates of wild-type Eph4 cells under iso- (Iso) and hypo-osmotic (Hypo) conditions, the latter treated with either DMSO or Torin-1 were resolved by SDS-PAGE and immunoblotted with indicated antibodies. **(D)** Quantification of C. $N = 3$ independent experiments; error bar, SD; **, $P = 0.0019$; ***, $P = 0.0002$; and ****, $P < 0.0001$ by one-way ANOVA with Tukey's post-hoc test. **(E)** Eph4 cells expressing a GFP-based fluorogenic caspase-3 reporter, FlipGFP(casp3)-T2A-mCherry (Zhang et al., 2019), were treated with either iso- (Iso) or hypo-osmotic (Hypo) buffer. Cells treated with anti-Fas-antibody serve as the positive control for apoptosis. Scale bar, 10 μm . **(F)** Quantification of the rate of cells that undergo apoptosis under the conditions described in E. $N = 3$ independent experiments; error bar, SD; ***, $P = 0.0003$ and ns, not significant by one-way ANOVA with Tukey's post-hoc test. **(G)** Wild-type Eph4 cells (WT), Rictor KD cells, and Rab35 KO cells were treated with hypo-osmotic buffer (30 mOsm/liter) for 30 min and stained with PI (red; nucleus of dead cells) and Calcein-AM (green; cytosol of live cells) to evaluate live and dead cells. Scale bar, 20 μm . **(H)** Quantification of the ratio of dead cells to total cells under the conditions described in G. $N = 5$ independent experiments; error bar, SD; ****, $P < 0.0001$ by one-way ANOVA with Tukey's post-hoc test. **(I)** Scanning electron microscopy wild-type Eph4 cells under iso-osmotic buffer (Iso) and wild-type (WT), Rictor KD and Rab35 KO cells treated with hypo-osmotic buffer (30 mOsm/liter) for 10 min. Scale bar, 10 μm . **(J)** Quantification of the ratio of live cells to total cells in Rictor KD cells stably expressing mScarlet only or mScarlet-Rab35 Q67L and stained with Calcein-AM. Cells were treated with hypo-osmotic buffer (30 mOsm/liter) for 40 min. $N = 5$ independent experiments; error bar, SD; ****, $P < 0.0001$ by Student's *t* test. This data is related to Videos 3 and 4. **(K)** Immunoblot of active, GTP-Rab35 purified by pull-down with the Rab-binding domain (RBD) of the Rab35 effector MICAL-3 in samples prepared from Eph4 cells stably expressing either wild-type or Q67L mScarlet-Rab35. Cells were maintained in iso-osmotic medium (-) and exposed to hypo-osmotic medium (Hypo, 150 mOsm/liter) for 2 min before lysis. **(L)** Quantification of K. $N = 3$ independent experiments; error bar, SD; *P* values indicated are from one-way ANOVA with Tukey's post-hoc test. Data from Q67L was considered as outliers and excluded from comparison. **(M)** Localization of the GFP-tagged RBD of MICAL-3 in wild-type Eph4 cells stably expressing wild-type mScarlet-Rab35 treated with DMSO (Control) or 250 nM Torin-1 for 24 h. Scale bar, 5 μm . **(N)** Quantification of M. $N = 3$ independent experiments; error bar, SD; *, $P = 0.0189$ by Student's *t* test. Source data are available for this figure: SourceData F7.

using TALON metal affinity resin (Clontech) as described previously (Ikenouchi et al., 2012). Bacterial sphingomyelinase (bSMase) from *Staphylococcus aureus* was purchased from Sigma-Aldrich. Myriocin (CAY 63150), Torin 1 (CAY 10997), and Ku-0063794 (CAY 13597) were obtained from Cayman Chemical. HPA-12 (H1553) was obtained from Tokyo Chemical Industry Co., Ltd.

The following primary antibodies were used for immunofluorescence microscopy and immunoblotting: mouse anti-Podocalyxin/GPI135 mAb (3F2/D8; Developmental Studies Hybridoma Bank); mouse anti-Caveolin-1 mAb (2297), mouse anti-GM130 mAb (610822; BD Transduction Laboratories); rabbit anti-Rictor pAb, rabbit anti-Akt (pan) mAb (C67E7), rabbit anti-phospho-Akt (Ser473) mAb (D9E; Cell Signaling Technology); mouse anti-GFP mAb (clones 7.1 and 13.1; Roche; for immunostaining); mouse anti-DYKDDDK tag mAb (1E6; Wako); and rat anti-E-cadherin (ECCD-2 mAbs; TaKaRa). Rat anti-GFP mAb (JFP-5), rabbit anti-RFP pAb and mouse anti- α -tubulin mAb (12G10) were produced in house.

Secondary antibodies were as follows: Cy2-conjugated donkey anti-rat-IgG antibody (712-225-150), anti-mouse-IgG antibody (715-225-151), and anti-rabbit-IgG antibody (711-225-152); Cy3-conjugated donkey anti-rat-IgG antibody (712-165-153), anti-mouse-IgG antibody (715-165-150), and anti-rabbit-IgG antibody (711-165-152) (Jackson ImmunoResearch Inc.); and HRP-conjugated anti-rat-IgG antibody (HAF005; R&D Systems), anti-mouse-IgG antibody (A90-516P; Bethyl Laboratories), and anti-rabbit-IgG antibody (4030-05; Southern Biotech). F-actin was visualized with either Alexa-Fluor-488 Phalloidin (A12379) or Alexa-Fluor-594 Phalloidin (A12381) (Invitrogen). Nucleus was visualized with 4',6-diamidino-2-phenylindole (DAPI; 049-18801; Wako Pure Chemical Industries). Eph4 cells were treated with anti-Fas antibody (SY-001) purchased from MBL, and cycloheximide was purchased from Sigma-Aldrich to induce apoptosis.

Inhibitor library screening

Inhibitor library was obtained from Screening Committee of Anticancer Drugs supported by Grant-in-Aid for Scientific Research on Innovative Areas, Scientific Support Programs for Cancer Research, from The Ministry of Education, Culture,

Sports, Science and Technology. Eph4 cells expressing SS-GFP-Lys are seeded at 1.0×10^4 cells/well on a 96 well glass-bottom plate, and after 12 h of incubation, each inhibitor is added to a final concentration of 20 μM . After treatment with each inhibitor for 24 h, the medium was changed to Hepes-buffered saline and the cells were observed at 37°C with a confocal microscope (LSM700; Carl Zeiss MicroImaging, Inc.) equipped with a Plan-APO objective (63/1.40 N.A. oil-immersion).

Fluorescence microscopy

Immunofluorescence microscopy was performed as described previously (Shiomi et al., 2015). In brief, cells cultured on coverslips were fixed with 3% formalin prepared in PBS for 10 min at RT, treated with 0.4% Triton X-100 prepared in PBS for 5 min, and washed with PBS. Fixed cells were blocked with 5% BSA prepared in PBS for 30 min at RT. Antibodies were diluted in this blocking solution. Cells were incubated with primary antibodies for 1 h at RT and with secondary antibodies for 30 min at RT. Specimens were observed at RT with a confocal microscope (LSM700; Carl Zeiss MicroImaging, Inc.) equipped with a Plan-APO objective (63/1.40 N.A. oil-immersion) with appropriate binning of pixels and exposure times. Images were analyzed with ZEN 2012 (Carl Zeiss MicroImaging, Inc.). To visualize the sub-cellular localization of sphingomyelin, living cells were stained with His-RFP-Lysenin or His-GFP-Lysenin prepared in serum-free DMEM and observed after washing out unbound protein with serum-free DMEM. NucBlue Live Ready Probes (R37605; Thermo Fisher Scientific) was used to stain the nuclei of live cells. All living cells were observed on a stage heater at 37°C or 20°C (Fig. S3 C).

Isolation of the apical membrane fraction

The apical membrane fraction was isolated from Eph4 cells using the method of Gerl et al. (2012). Briefly, the apical membrane was physically isolated from cultured epithelial cells using a nitrocellulose membrane.

Lipid analysis

Cells were cultured to confluence in a 100-mm diameter plastic dish, and total lipids were extracted by Bligh and Dyer method.

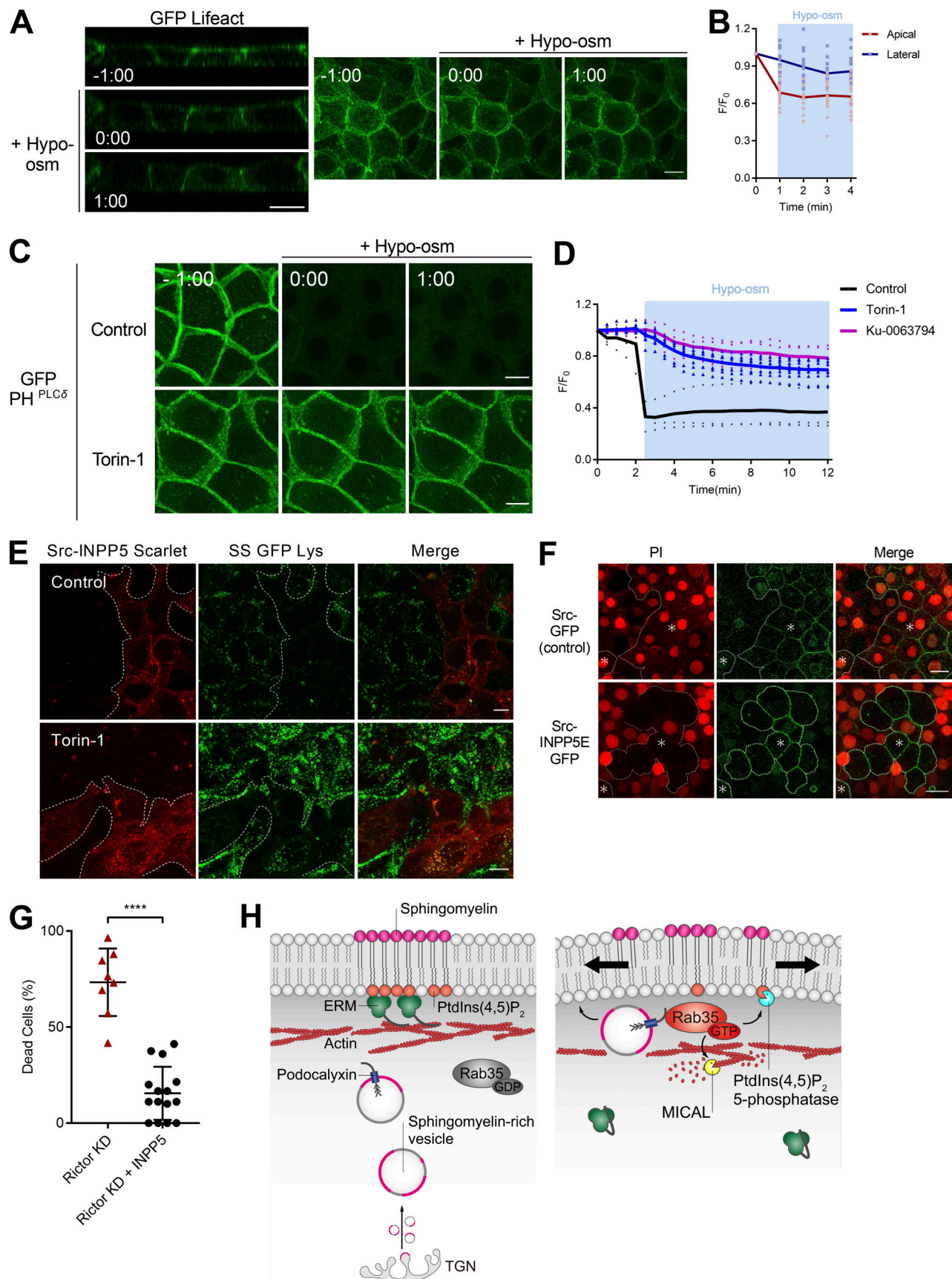


Figure 8. **Reduction of PI(4,5)P₂ by the activation of mTORC2-Rab35 axis is essential for the adaptation to hypo-osmotic stress.** (A and B) Time-lapse imaging and quantification of EpH4 cells stably expressing GFP-Lifect. Hypo-osmotic buffer (150 mOsm/liter) was added at time 0:00. Fluorescence

intensities at apical membranes and basolateral membranes normalized to the value at $t = 0$ min and shown as the mean line. Scale bar, 10 μm . $N = 15$ independent experiments. **(C and D)** Time-lapse imaging and quantification of Eph4 cells stably expressing GFP-PH^{PLC β} . hypo-osmotic buffer (150 mOsm/liter) was added at time 0:00. The decrease of GFP-PH^{PLC β} signal in the apical membrane due to hypotonic stress was suppressed by the treatment with either 250 nM Torin-1 or 3 μM Ku-0063794 for 24 h. Scale bar, 10 μm . Fluorescence intensities normalized to the value at $t = 0$ min and shown as the mean line. $N \geq 3$ independent experiments. **(E)** Eph4 cells expressing SS-GFP-Lys and Src-INPP5E-Scarlet were treated with DMSO (Control) or 250 nM Torin-1 for 24 h. Scale bar, 10 μm . **(F and G)** Representative images and quantification of Rictor KD cells expressing Src-GFP (control) vector or Src-INPP5E-GFP were treated with hypo-osmotic buffer (30 mOsm/liter) for 30 min and stained with PI (red; nucleus of dead cells) and NucBlue (total cell). $N \geq 8$ independent experiments; error bar, SD; ***, $P < 0.0001$ by Student's t test. **(H)** mTORC2 and Rab35 buffer plasma membrane tension by reducing the actin cortex and increasing transport of apical membrane components in order to protect against cell death by rupturing during hypo-osmotic challenge.

Briefly, after the medium was washed several times with ice-cold PBS, cells were scraped from the plastic dish with 2 ml of methanol using a cell scraper, and 1 ml of chloroform and 0.8 ml of ultra-pure water were added to methanol and mixed well. Thereafter, 1 ml of chloroform and 1 ml of ultra-pure water were added, mixed well, and centrifuged to separate a chloroform layer. The concentration of total phospholipid was estimated by phosphorus determination through an acidic digestion. For the quantification of sphingomyelin, Sphingomyelin Assay Kit (STA-601; CBL Cell Biolabs, Inc.) was used.

Lumen formation of MDCK II cells

MDCK cysts were grown in 3D Matrigel cultures (BD), as described previously (Bryant et al., 2010). Drugs were added at the indicated final concentrations at the time of cell seeding. Cells were grown for 6–48 h before fixation in 4% paraformaldehyde. The number of cysts with a single lumen or multiple lumens was measured and quantified as a percentage of the total number of measurements.

Cell viability assay

After applying hypo-osmotic stress (diluted HBSS by a factor of 10; 30 mOsm/liter) for 15 min, the cells were stained using Cellstain Double Staining Kit following the manufacturer's instructions. The total period of exposure to hypo-osmotic stress was designed to be 30 min. The cytoplasmic green fluorescence signals of Calcein-AM were observed only in the living cells. On the other hand, the red fluorescence of propidium iodide (PI) signal indicates dead cells.

Rab35 activity assays

Lysates from Eph4 cells stably expressing either WT or Q67L mScarlet-Rab35 and from HEK293 cells transiently expressing FLAG-MICAL3-RBD were prepared in lysis buffer (50 mM HEPES-NaOH pH 7.5, 150 mM NaCl, 10 mM MgCl₂, 1% NP-40, 5% glycerol) and incubated with anti-DYKDDDK tag antibody beads (Wako, 018-2783) for 40 min. The beads were washed three times in lysis buffer and the bound proteins were eluted in SDS sample buffer. Samples were analyzed by immunoblotting with anti-RFP pAb and anti-DYKDDDK tag mAb.

Online supplemental material

Fig. S1 shows changes in subcellular localization of caveolins after hypo-osmotic stress. Fig. S2 shows co-localization of SS-GFP-Lys containing vesicles with various organelle marker proteins. Fig. S3 shows that inhibition of mTORC2 activity did

not affect the biosynthesis of sphingomyelin or the formation of transport vesicles of sphingomyelin from TGN. Fig. S4 shows that mTORC2 plays essential roles in the epithelial cyst formation by promoting apical transport of vesicles containing sphingomyelin and podocalyxin. Fig. S5 shows that depletion of Rab35 affects the apical transport of sphingomyelin. Video 1 shows that exposure to hypo-osmotic medium causes cell rupture in Rictor KD cells. Video 2 shows that the overexpression of Scarlet-Rab35-Q67L suppresses cell death of Rictor KD cells exposed to hypo-osmotic medium. Video 3 shows that treatment with hypo-osmotic medium rapidly reduces the actin cortex of the apical membrane. Video 4 shows that treatment with hypo-osmotic medium leads to the reduction of PI(4,5)P₂ at the apical membrane.

Acknowledgments

We thank all members of the Ikenouchi laboratory (Department of Biology, Faculty of Sciences, Kyushu University) for helpful discussions.

This work was supported by JSPS KAKENHI (JP19H03227 [J. Ikenouchi], JP21K19231 [J. Ikenouchi], JP19K06640 [K. Matsuzawa], and JP20J10229 [Y. Ono]), AMED-FORCE (21gm4010011h0001), JST-FORCE (JPMJFR204L) and grants from the Mitsubishi Foundation, the Cell Science Research Foundation and a JSPS Research Fellowship for Young Scientists (DC2; Y. Ono).

The authors declare no competing financial interests.

Author contributions: Y. Ono performed most of the experiments and analyzed the data. K. Matsuzawa performed some experiments. J. Ikenouchi designed the research and wrote the paper.

Submitted: 25 June 2021

Revised: 28 December 2021

Accepted: 24 January 2022

References

- Berchtold, D., M. Piccolis, N. Chiaruttini, I. Riezman, H. Riezman, A. Roux, T.C. Walther, and R. Loewith. 2012. Plasma membrane stress induces relocation of Slm proteins and activation of TORC2 to promote sphingolipid synthesis. *Nat. Cell Biol.* 14:542–547. <https://doi.org/10.1038/ncb2480>
- Berchtold, D., and T.C. Walther. 2009. TORC2 plasma membrane localization is essential for cell viability and restricted to a distinct domain. *Mol. Biol. Cell.* 20:1565–1575. <https://doi.org/10.1091/mbc.e08-10-1001>
- Bryant, D.M., A. Datta, A.E. Rodríguez-Fraticelli, J. Peränen, F. Martín-Belmonte, and K.E. Mostov. 2010. A molecular network for de novo generation of the apical surface and lumen. *Nat. Cell Biol.* 12:1035–1045. <https://doi.org/10.1038/ncb2106>

- Bryant, D.M., J. Roignot, A. Datta, A.W. Overeem, M. Kim, W. Yu, X. Peng, D.J. Eastburn, A.J. Ewald, Z. Werb, and K.E. Mostov. 2014. A molecular switch for the orientation of epithelial cell polarization. *Dev. Cell.* 31: 171–187. <https://doi.org/10.1016/j.devcel.2014.08.027>
- Dai, J., and M.P. Sheetz. 1995. Regulation of endocytosis, exocytosis, and shape by membrane tension. *Cold Spring Harb. Symp. Quant. Biol.* 60: 567–571. <https://doi.org/10.1101/sqb.1995.060.01.060>
- Dambournet, D., M. Machicoane, L. Chesneau, M. Sachse, M. Rocancourt, A. El Marjou, E. Formstecher, R. Salomon, B. Goud, and A. Echard. 2011. Rab35 GTPase and OCRL phosphatase remodel lipids and F-actin for successful cytokinesis. *Nat. Cell Biol.* 13:981–988. <https://doi.org/10.1038/ncb2279>
- Deng, Y., F.E. Rivera-Molina, D.K. Toomre, and C.G. Burd. 2016. Sphingomyelin is sorted at the trans Golgi network into a distinct class of secretory vesicle. *Proc. Natl. Acad. Sci. USA.* 113:6677–6682. <https://doi.org/10.1073/pnas.1602875113>
- Diz-Muñoz, A., K. Thurley, S. Chintamen, S.J. Altschuler, L.F. Wu, D.A. Fletcher, and O.D. Weiner. 2016. Membrane tension acts through PLD2 and mTORC2 to limit actin network assembly during neutrophil migration. *PLoS Biol.* 14:e1002474. <https://doi.org/10.1371/journal.pbio.1002474>
- Frémont, S., H. Hammich, J. Bai, H. Wioland, K. Klinkert, M. Rocancourt, C. Kikuti, D. Stroebel, G. Romet-Lemonne, O. Pylypenko, A. Houdusse, et al. 2017. Oxidation of F-actin controls the terminal steps of cytokinesis. *Nat. Commun.* 8:14528. <https://doi.org/10.1038/ncomms14528>
- Fukuda, M., E. Kanno, K. Ishibashi, and T. Itoh. 2008. Large scale screening for novel rab effectors reveals unexpected broad Rab binding specificity. *Mol. Cell. Proteomics.* 7:1031–1042. <https://doi.org/10.1074/mcp.M700569-MCP200>
- Futerman, A.H., B. Stieger, A.L. Hubbard, and R.E. Pagano. 1990. Sphingomyelin synthesis in rat liver occurs predominantly at the cis and medial cisternae of the Golgi apparatus. *J. Biol. Chem.* 265:8650–8657
- Gerl, M.J., J.L. Sampaio, S. Urban, L. Kalvodova, J.M. Verbavatz, B. Binnington, D. Lindemann, C.A. Lingwood, A. Shevchenko, C. Schroeder, and K. Simons. 2012. Quantitative analysis of the lipidomes of the influenza virus envelope and MDCK cell apical membrane. *J. Cell Biol.* 196:213–221. <https://doi.org/10.1083/jcb.201108175>
- Grahammer, F., S.K. Ramakrishnan, M.M. Rinschen, A.A. Larionov, M. Syed, H. Khatib, M. Roerden, J.O. Sass, M. Helmstaedter, D. Osenberg, L. Kühne, et al. 2017. mTOR regulates endocytosis and nutrient transport in proximal tubular cells. *J. Am. Soc. Nephrol.* 28:230–241. <https://doi.org/10.1681/ASN.201511224>
- Guertin, D.A., D.M. Stevens, C.C. Thoreen, A.A. Burds, N.Y. Kalaany, J. Moffat, M. Brown, K.J. Fitzgerald, and D.M. Sabatini. 2006. Ablation in mice of the mTORC components raptor, rictor, or mLST8 reveals that mTORC2 is required for signaling to Akt-FOXO and PKCalpha, but not S6K1. *Dev. Cell.* 11:859–871. <https://doi.org/10.1016/j.devcel.2006.10.007>
- Ikenouchi, J., M. Hirata, S. Yonemura, and M. Umeda. 2013. Sphingomyelin clustering is essential for the formation of microvilli. *J. Cell Sci.* 126: 3585–3592. <https://doi.org/10.1242/jcs.122325>
- Ikenouchi, J., M. Suzuki, K. Umeda, K. Ikeda, R. Taguchi, T. Kobayashi, S.B. Sato, T. Kobayashi, D.B. Stolz, and M. Umeda. 2012. Lipid polarity is maintained in absence of tight junctions. *J. Biol. Chem.* 287:9525–9533. <https://doi.org/10.1074/jbc.M111.327064>
- Janmey, P.A., R. Bucki, and R. Radhakrishnan. 2018. Regulation of actin assembly by PI(4,5)P2 and other inositol phospholipids: an update on possible mechanisms. *Biochem. Biophys. Res. Commun.* 506:307–314. <https://doi.org/10.1016/j.bbrc.2018.07.155>
- Kiyokawa, E., A. Makino, K. Ishii, N. Otsuka, A. Yamaji-Hasegawa, and T. Kobayashi. 2004. Recognition of sphingomyelin by lysenin and lysenin-related proteins. *Biochemistry.* 43:9766–9773. <https://doi.org/10.1021/bi049561j>
- Klinkert, K., M. Rocancourt, A. Houdusse, and A. Echard. 2016. Rab35 GTPase couples cell division with initiation of epithelial apico-basal polarity and lumen opening. *Nat. Commun.* 7:11166. <https://doi.org/10.1038/ncomms11166>
- Kozera, L., E. White, and S. Calaghan. 2009. Caveolae act as membrane reserves which limit mechanosensitive I(Cl,swell) channel activation during swelling in the rat ventricular myocyte. *PLoS One.* 4:e8312. <https://doi.org/10.1371/journal.pone.0008312>
- Le Roux, A.L., X. Quiroga, N. Walani, M. Arroyo, and P. Roca-Cusachs. 2019. The plasma membrane as a mechanochemical transducer. *Philos. Trans. R. Soc. Lond. B Biol. Sci.* 374:20180221. <https://doi.org/10.1098/rstb.2018.0221>
- Liu, G.Y., and D.M. Sabatini. 2020. mTOR at the nexus of nutrition, growth, ageing and disease. *Nat. Rev. Mol. Cell Biol.* 21:183–203. <https://doi.org/10.1038/s41580-019-0199-y>
- Martin-Belmonte, F., A. Gassama, A. Datta, W. Yu, U. Rescher, V. Gerke, and K. Mostov. 2007. PTEN-mediated apical segregation of phosphoinositides controls epithelial morphogenesis through Cdc42. *Cell.* 128: 383–397. <https://doi.org/10.1016/j.cell.2006.11.051>
- Meder, D., A. Shevchenko, K. Simons, and J. Füllekrug. 2005. Gp135/podocalyxin and NHERF-2 participate in the formation of a preapical domain during polarization of MDCK cells. *J. Cell Biol.* 168:303–313. <https://doi.org/10.1083/jcb.200407072>
- Mrozowska, P.S., and M. Fukuda. 2016. Regulation of podocalyxin trafficking by Rab small GTPases in 2D and 3D epithelial cell cultures. *J. Cell Biol.* 213:355–369. <https://doi.org/10.1083/jcb.201512024>
- Muir, A., S. Ramachandran, F.M. Roelants, G. Timmons, and J. Thorner. 2014. TORC2-dependent protein kinase Ypk1 phosphorylates ceramide synthase to stimulate synthesis of complex sphingolipids. *Elife.* 3:e03779. <https://doi.org/10.7554/eLife.03779>
- Niles, B.J., H. Mogri, A. Hill, A. Vlahakis, and T. Powers. 2012. Plasma membrane recruitment and activation of the AGC kinase Ypk1 is mediated by target of rapamycin complex 2 (TORC2) and its effector proteins Slm1 and Slm2. *Proc. Natl. Acad. Sci. USA.* 109:1536–1541. <https://doi.org/10.1073/pnas.1117563109>
- Pietuch, A., B.R. Brückner, and A. Janshoff. 2013. Membrane tension homeostasis of epithelial cells through surface area regulation in response to osmotic stress. *Biochim. Biophys. Acta.* 1833:712–722. <https://doi.org/10.1016/j.bbamcr.2012.11.006>
- Pontes, B., P. Monzo, and N.C. Gauthier. 2017. Membrane tension: a challenging but universal physical parameter in cell biology. *Semin. Cell Dev. Biol.* 71:30–41. <https://doi.org/10.1016/j.semcdb.2017.08.030>
- Rai, A., A. Oprisko, J. Campos, Y. Fu, T. Friesse, A. Itzen, R.S. Goody, E.M. Gazdag, and M.P. Müller. 2016. bMERB domains are bivalent Rab8 family effectors evolved by gene duplication. *Elife.* 5:e18675. <https://doi.org/10.7554/eLife.18675>
- Riggi, M., K. Niewola-Staszewska, N. Chiaruttini, A. Colom, B. Kusmider, V. Mercier, S. Soleimanpour, M. Stahl, S. Matile, A. Roux, and R. Loewith. 2018. Decrease in plasma membrane tension triggers PtdIns(4,5)P(2) phase separation to inactivate TORC2. *Nat. Cell Biol.* 20:1043–1051. <https://doi.org/10.1038/s41556-018-0150-z>
- Roelants, F.M., D.K. Breslow, A. Muir, J.S. Weissman, and J. Thorner. 2011. Protein kinase Ypk1 phosphorylates regulatory proteins Orm1 and Orm2 to control sphingolipid homeostasis in *Saccharomyces cerevisiae*. *Proc. Natl. Acad. Sci. USA.* 108:19222–19227. <https://doi.org/10.1073/pnas.1116948108>
- Shiomi, R., K. Shigetomi, T. Inai, M. Sakai, and J. Ikenouchi. 2015. CaMKII regulates the strength of the epithelial barrier. *Sci. Rep.* 5:13262. <https://doi.org/10.1038/srep13262>
- Sinha, B., D. Köster, R. Ruez, P. Gonnord, M. Bastiani, D. Abankwa, R.V. Stan, G. Butler-Browne, B. Védie, L. Johannes, N. Morone, et al. 2011. Cells respond to mechanical stress by rapid disassembly of caveolae. *Cell.* 144: 402–413. <https://doi.org/10.1016/j.cell.2010.12.031>
- Strilić, B., T. Kucera, J. Eglinger, M.R. Hughes, K.M. McNagny, S. Tsukita, E. Dejana, N. Ferrara, and E. Lammert. 2009. The molecular basis of vascular lumen formation in the developing mouse aorta. *Dev. Cell.* 17: 505–515. <https://doi.org/10.1016/j.devcel.2009.08.011>
- Yamaji, A., Y. Sekizawa, K. Emoto, H. Sakuraba, K. Inoue, H. Kobayashi, and M. Umeda. 1998. Lysenin, a novel sphingomyelin-specific binding protein. *J. Biol. Chem.* 273:5300–5306. <https://doi.org/10.1074/jbc.273.9.5300>
- Yang, J., X. Zhao, A. Patel, R. Potru, S. Azizi-Ghannad, M. Dolinger, J. Cao, C. Bartholomew, J. Mazurkiewicz, D. Conti, D. Jones, et al. 2015. Rapamycin inhibition of mTOR reduces levels of the Na⁺/H⁺ exchanger 3 in intestines of mice and humans, leading to diarrhea. *Gastroenterology.* 149:151–162. <https://doi.org/10.1053/j.gastro.2015.03.046>
- Zhang, Q., A. Schepis, H. Huang, J. Yang, W. Ma, J. Torra, S.Q. Zhang, L. Yang, H. Wu, S. Nonell, Z. Dong, et al. 2019. Designing a green fluorogenic protease reporter by flipping a beta strand of GFP for imaging apoptosis in animals. *J. Am. Chem. Soc.* 141:4526–4530. <https://doi.org/10.1021/jacs.8b13042>

Supplemental material

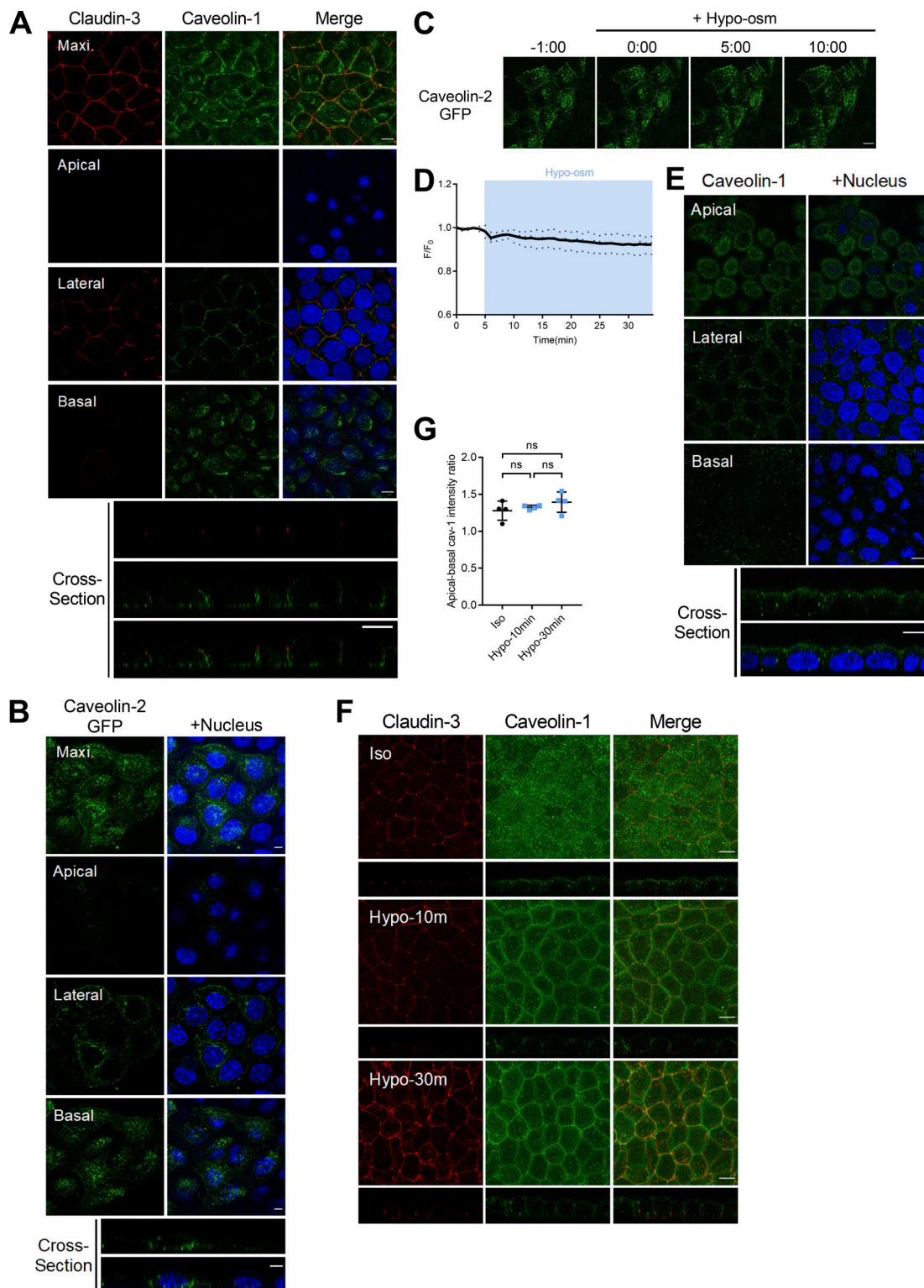


Figure S1. **Changes of subcellular localization of caveolins after hypo-osmotic stress (related to Fig. 1).** (A) Wild-type EpH4 cells stained with anti-Claudin-3 pAb and anti-Caveolin-1 mAb. The lower panels show the snapshots in the z-axis direction. Scale bar, 10 μ m. (B) Wild-type EpH4 cells stably expressed cGFP-tagged Caveolin-2. The lower pictures show the snapshot in the z-axis direction. Scale bar, 5 μ m. (C) Time-lapse imaging of EpH4 cells stably expressing Caveolin-2-GFP. Hypo-osmotic buffer (150 mOsm/liter) was added at time 0:00. Scale bar, 5 μ m. (D) Fluorescence intensities normalized to the value at $t = 0$ min and shown as the mean line. $N = 3$ independent experiments. (E) Wild-type MDCK cells stained with anti-Caveolin-1 mAb. The lower panels show the snapshots in the z-axis direction. Scale bar, 10 μ m. (F) Wild-type MDCK cells treated with hypo-osmotic buffer (150 mOsm/liter) for indicated time were fixed and stained with anti-Claudin-3 pAb and anti-Caveolin mAb. Scale bar, 10 μ m. (G) Quantification of the ratio of fluorescence signal of caveolin-1 staining of the apical membrane to that of the basolateral membrane in wild-type MDCK cells treated with hypo-osmotic buffer (150 mOsm/liter) for indicated time. $N = 4$ independent experiments; error bar, SD; ns, not significant by one-way ANOVA with Tukey's post-hoc test.

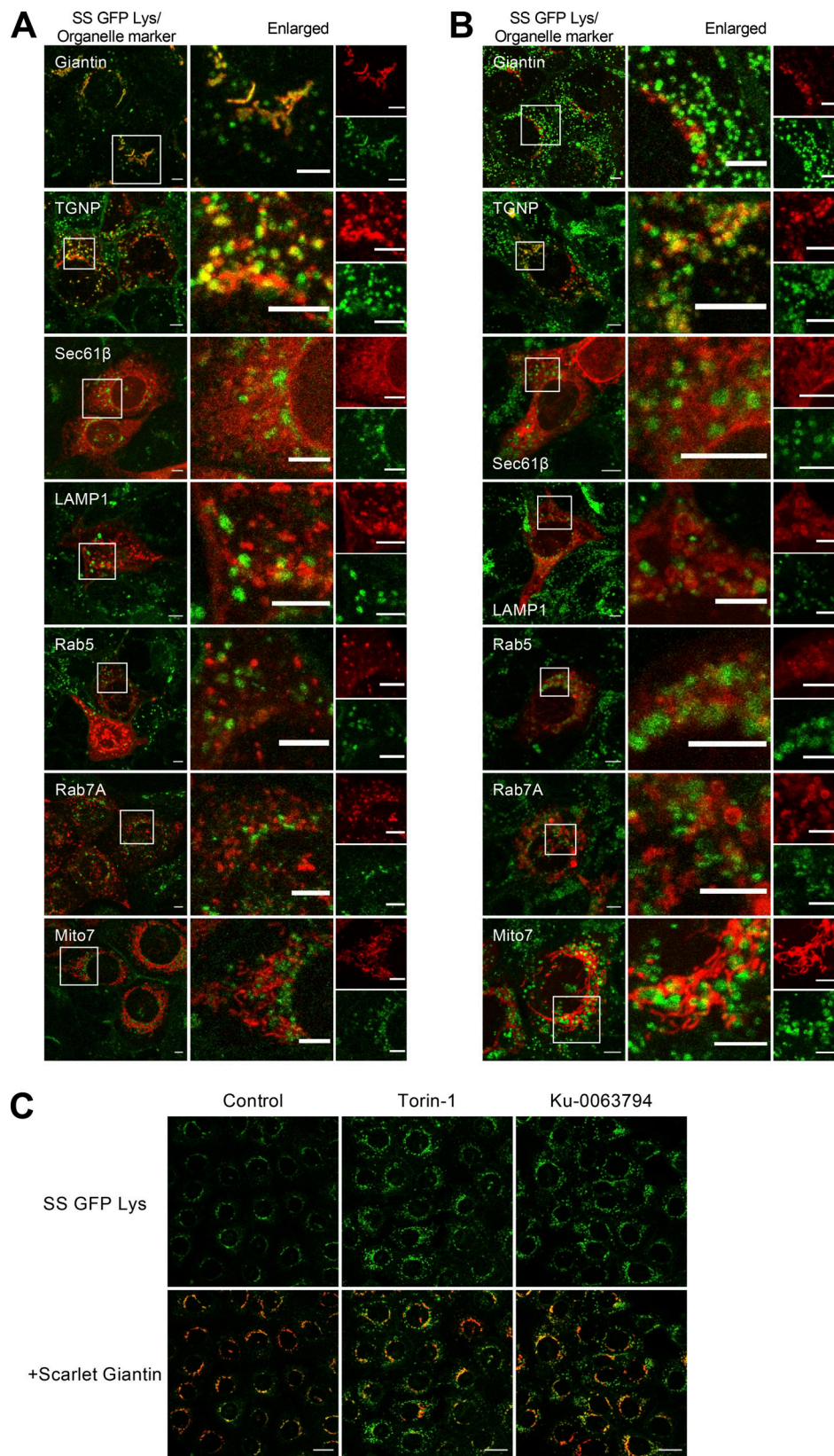


Figure S2. **Examination of co-localization of SS-GFP-Lys containing vesicles with various organelle marker proteins (related to Fig. 3 and Fig. 4).** **(A)** EpH4 cells expressing SS-GFP-Lys were transfected with mScarlet-Giantin, mCherry-TGNP, mCherry-Sec61β, mRFP-LAMP1, mCherry-Rab5, mCherry-Rab7A and mCherry-Mito-7 expression vectors. Scale bar, 5 μm. **(B)** EpH4 cells expressing SS-GFP-Lys and the proteins as described in A were treated with 250 nM Torin-1 for 24 h. Scale bar, 5 μm. **(C)** Treatment with inhibitors of mammalian target of rapamycin signal pathway increased the number of SS-GFP-Lys positive vesicles. Low magnification images of Fig. 4 A. Scale bar, 10 μm.

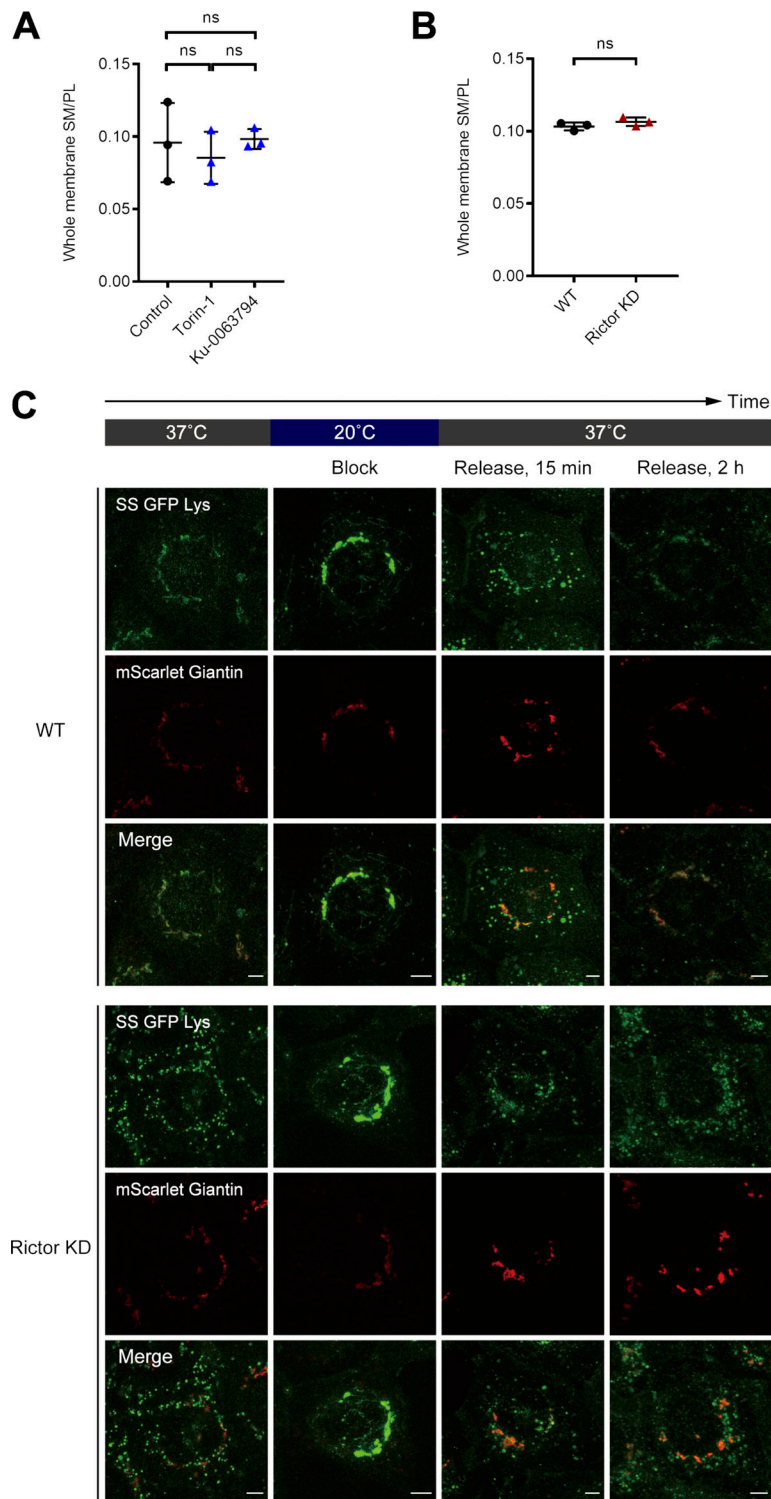


Figure S3. **Loss of mTORC2 activity did not affect biosynthesis of sphingomyelin or formation of transport vesicles of sphingomyelin from TGN (related to Fig. 4).** **(A)** Wild-type Eph4 cells were treated with DMSO (Control), 250 nM Torin-1 (mTOR inhibitor) or 3 μ M Ku-0063794 (mTOR inhibitor) for 72 h. Total cellular lipids were extracted by Bligh and Dyer method. The total amount of phospholipid (mM) and the amount of sphingomyelin (mg/dl) were quantified. $N = 3$ independent experiments; error bar, SD; *, $P = 0.0140$; and ns, not significant by one-way ANOVA with Tukey's post-hoc test. **(B)** Total phospholipids of wild type Eph4 cells (WT) and Rictor KD cells were extracted by Bligh and Dyer method. Total amount of phospholipids (mM) and the amount of sphingomyelin (mg/dl) were quantified. $N = 3$ from independent experiments; error bar, SD; ns, not significant by Student's t test. **(C)** Wild-type Eph4 cells (WT) and Rictor KD cells (Rictor KD) co-expressing SS-GFP-Lys and mScarlet-mGiantin were cultured at 20°C for 2 h to block export from the TGN. This incubation resulted in depletion of cytoplasmic signals of SS-GFP-Lys and accumulation of SS-GFP-Lys in the Golgi apparatus. Release of the 20°C block by incubating the cells at 37°C for just 15 min resulted in the reappearance of SS-GFP-Lys containing vesicles in the cytoplasm. No significant difference was observed in the number of SS-GFP-Lys positive vesicles from Golgi bodies between wild-type Eph4 cells and Rictor KD cells. Scale bar, 5 μ m.

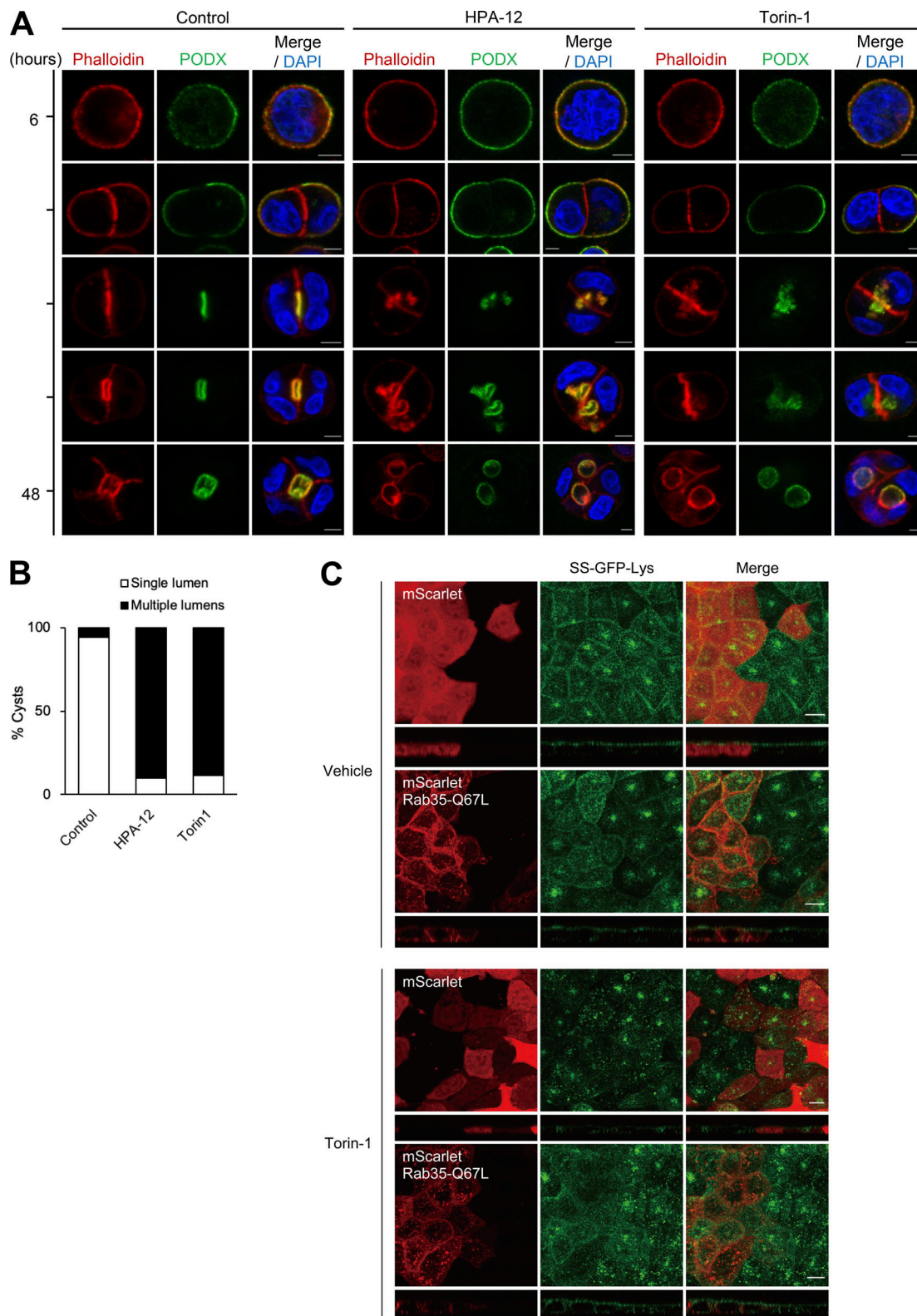


Figure S4. **mTORC2 plays essential roles in the epithelial cyst formation by promoting apical transport of vesicles containing sphingomyelin and podocalyxin.** (A) Representative immunofluorescence images showing development of apical lumen in wild-type MDCK cysts incubated with DMSO (Control), 40 μ M HPA-12 or 1 μ M Torin-1. After plating indicated time, cysts were fixed and stained with phalloidin (red), mAb against GP135/podocalyxin (green) and DAPI (blue). Scale bar, 5 μ m. (B) Quantification of cysts with normal lumens or multiple lumens in cells treated with indicated inhibitors at 48 h. (Control, $N = 490$; HPA-12, $N = 507$; Torin-1, $N = 510$ cysts from five independent experiments). (C) EpH4 cells stably expressing GFP-podocalyxin were transfected with mScarlet only or mScarlet-tagged-Rab35 dominant active mutant (Q67L) expression vectors and treated with 250 nM Torin-1 or 3 μ M Ku-0063794 for 24 h. Transfected cells are indicated by the white-dotted line. Scale bar, 10 μ m.

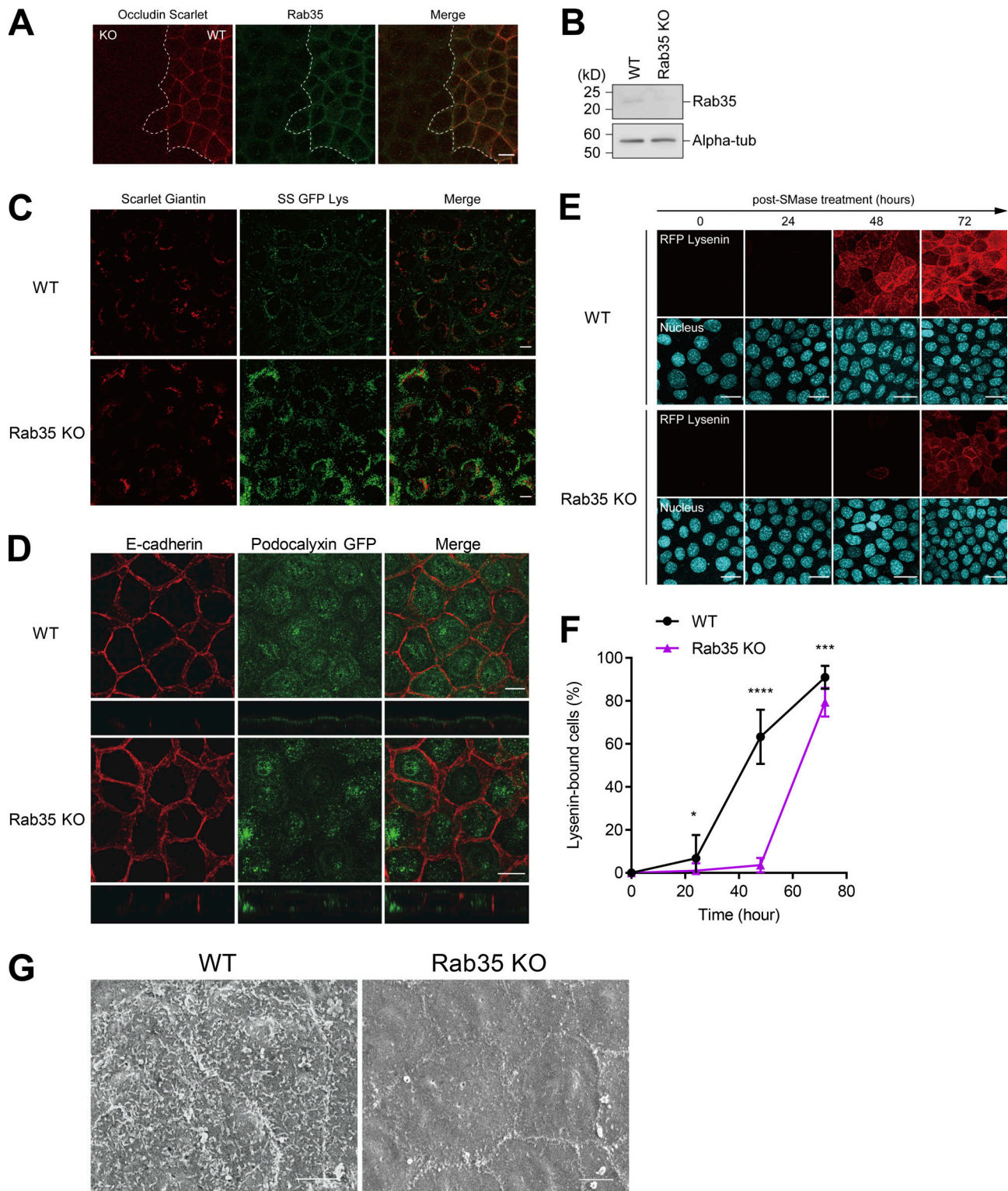


Figure S5. **Rab35 is required for the apical transport of sphingomyelin.** (A) Wild-type Eph4 cells stably expressing Scarlet-Occludin and Rab35 KO cells were cultured together and stained with anti-Rab35 antibody (Green). Scale bar, 10 μ m. (B) Total cell lysate of Rab35 KO cells was resolved by SDS-PAGE and immunoblotted with anti-Rab35 mAb and anti-alpha-tubulin mAb. (C) Subcellular localization of SS-GFP-Lys expressed in wild-type Eph4 cells and Rab35 KO cells. Scale bar, 10 μ m. (D) Subcellular localization of GFP-tagged podocalyxin expressed in wild-type Eph4 cells and Rab35 KO cells. Scale bar, 10 μ m. (E) Eph4 wild-type (WT) cells and Rab35 KO cells were treated with bSMase. bSMase was washed out and cells were cultured in normal medium for the indicated times. Recovery of sphingomyelin at the apical membrane was evaluated by staining with RFP-Lysenin. Scale bar, 20 μ m. (F) Quantification of the number of RFP-Lysenin-positive cells at the apical membrane based on E. $N \geq 12$ independent experiments; error bar, SD; *, $P = 0.1008$; ***, $P = 0.0001$; and ****, $P < 0.0001$ by Student's t test. (G) Scanning electron microscopy of wild-type Eph4 cells and Rab35 KO cells. Scale bar, 5 μ m. Source data are available for this figure: SourceData F55.

Video 1. **Exposure to hypo-osmotic medium causes cell death by rupturing in Rictor KD cells.** (Related to Fig. 7 J) Time-lapse imaging of cells stained with Calcein-AM after co-culture of Rictor KD EpH4 cells and Rictor KD cells stably expressing mScarlet only. Hypo-osmotic buffer (30 mOsm/liter) was added at time 0:00. Frames were taken every 2 min. Scale bar, 5 μ m.

Video 2. **Over-expression of Rab35-Q67L suppresses cell death of Rictor KD cells exposed to hypo-osmotic medium.** (Related to Fig. 7 J). Time-lapse imaging of cells stained with Calcein-AM after co-culture of Rictor KD EpH4 cells and Rictor KD cells stably expressing mScarlet-Rab35 Q67L. Hypo-osmotic buffer (30 mOsm/liter) was added at time 0:00. Frames were taken every 2 min. Scale bar, 5 μ m.

Video 3. **Treatment with hypo-osmotic medium rapidly reduces the actin cortex of the apical membrane.** (Related to Fig. 8 A) Time-lapse imaging of EpH4 cells stably expressing GFP-Lifeact. Hypo-osmotic buffer (150 mOsm/l) was added at time 0:00. Frames were taken every 30 s. Scale bar, 10 μ m.

Video 4. **Treatment with hypo-osmotic medium leads to the reduction of PI(4,5)P2 at the apical membrane.** (Related to Fig. 8 C) Time-lapse imaging of EpH4 cells stably expressing GFP-PH^{PLC δ} . Hypo-osmotic buffer (150 mOsm/l) was added at time 0:00. Frames were taken every 30 s. Scale bar, 10 μ m.